REPUBLIQUE ALGERIENNE DEMOCRATIQUE ET POPULAIRE

MINISTERE DE LENSIGNEMENT SUPERIEURE ET DE LA RECHERCHE SCIENTIFIQUE

Ecole Nationale Polytechnique

المدرسة الوطنية المتعددة التقنيات
Ecole Nationale Polytechnique

Département d'Electronique

Projet de fin d'études

Pour l'obtention du diplôme

D'Ingénieur d'Etat en Electronique

Présenté par:

BOUCHENAK-KHELLADI Anes

Thème :

TUNNEL JUNCTION BASED MEMORIES

M. Mourad HADDADI	**Professeur**	**ENP**	**Encadreur**
M. Weisheng ZHAO	**Docteur**	**IEF (Paris-Sud)**	**Responsable de stage**
M. Jacques-Olivier KLEIN	**Professeur**	**IEF (Paris-Sud)**	**Coresponsable de stage**

Soutenue le 24 Juin 2012 devant les membres du jury :

M. Hicham BOUSBIA-SALAH	**Docteur**	**ENP**	**Président**
M. Salah AIT-CHEIKH	**Docteur**	**ENP**	**Examinateur**
M. Mourad HADDADI	**Professeur**	**ENP**	**Rapporteur**

JUIN 2012

Ecole Nationale Polytechnique, 10 Avenue HASSEN BADI, El-Harrch, Alger

PEOPLE'S DEMOCRATIC REPUBLIC OF ALGERIA

MINISTRY OF HIGHER EDUCATION AND SCIENTIFIC RESEARCH

NATIONAL POLYTECHNIC SCHOOL

المدرسة الوطنية المتعددة التقنيات
Ecole Nationale Polytechnique

Electronics Department

Final Studies Project

To obtain

Electronics Engineer Diploma

Presented by:

BOUCHENAK KHELLADI Anes

Topic:

TUNNEL JUNCTION BASED MEMORIES

M. Mourad HADDADI	Professor	ENP	Supervisor
M. Weisheng ZHAO	Doctor	IEF (Paris-Sud)	Internship advisor
M. Jacques-Olivier KLEIN	Professor	IEF (Paris-Sud)	Internship co-advisor

Submitted June 24 th, 2012. Members of the jury:

M. Hicham BOUSBIA-SALAH	Doctor	ENP	President
M. Salah AIT-CHEIKH	Doctor	ENP	Examiner
M. Mourad HADDADI	Professor	ENP	Supervisor

JUNE 2012

ملخص

في عالمنا اليوم و التقدم المتواصل خاصة في مجال الإلكترونيك عدة أجهزة و منها الكمبيوتر تحتاج إلى تخزين بيانات ثنائية بطريقة دائمة أو نصف دائمة. هنا تأتي الذاكرة و التي تمثل عنصر من هذه الأجهزة لتقوم بتخزين المعلومات و بشكل واسع.

أثار البحث عن تكنولوجيا تحتفظ بهذه المعلومات بطريقة مستمرة و بكثافة كبيرة، ذات سرعة عالية سواء عند الكتابة أو القراءة و باستهلاك ضعيف للطاقة اهتماما كبيرا عند الباحثين لإيجاد مواد مكنز مات و تخطيطات جديدة.

من بين هذه الذاكرات الناجحة و الناجمة عن جهود كبيرة نذكر: الإنقلاب الذري،الRAM المقاومية وأخيرا الوصلة النفقية المغناطيسية.

ألحظ الباحثون في هذا المجال تقدما لافتا للوصول إلى ذاكرات غير متطايرة مبنية على وصلة نفقية بعازل كهربائي شفاف قادرة على تحقيق تسجيل باستهلاك جد ضعيف للطاقة و بطريقة مخلصة.

الكلمات المفتاحية : ذاكرات غير متطايرة، RAM، لولبية، الوصلة النفقية، حديد مغناطيسية، حديد إلكترونية، عازل.

ABSTRACT

Computers and other types of systems require the permanent or semi-permanent storage of large amounts of binary data and Memory is the portion of these systems which do it and in large quantities.

The quest for a non-volatile memory technology that offers high storage density, high read and writes speeds, and low power consumption has triggered intense research into new materials, mechanisms and device architectures.

The successful memory technologies emerging from these efforts have been the atomic switch, the resistive RAM and the magnetic tunnel junction.

Researchers in this domain report a substantial advance in an alternative approach to non-volatile memory technology based on ferroelectric tunnel junctions achieving very low write powers, in a highly reproducible manner.

Key words: Non-volatile memories, RAMs, Tunnel Junctions, spintronics, Ferromagnetic, Ferroelectric, Insulator.

RESUME

Les ordinateurs et d'autres types de systèmes exigent le stockage permanent ou semi-permanent des grandes quantités de données binaires et la Mémoire est la partie de ces systèmes qui le fait et en grandes quantités.

La quête pour une technologie de mémoires non-volatile qui offre une grande densité de stockage, une grande vitesse de lecture et d'écriture, et une faible consommation d'énergie a déclenché la recherche intense dans de nouveaux matériaux, de nouveaux mécanismes et de nouvelles d'architectures de dispositif.

Les technologies de mémoire réussies apparaissant de ces efforts ont été l'échange atomique, la RAM résistive et la jonction tunnel magnétique.

Les chercheurs dans ce domaine rapportent qu'une avance substantielle dans une approche alternative à la technologie de mémoire non volatile basée sur des jonctions tunnels ferroélectriques réalisant des cycles d'écriture avec une très faible consommation d'énergie et d'une façon très fiable et reproductible.

Mots Clés: Mémoires Non-volatiles, RAMs, Jonctions Tunnels, spintroniques, Ferromagnétique, Ferroélectrique, Isolant.

ACKNOWLEDGMENTS

Many people have provided me with assistance, guidance and support while I was working on my thesis.

First, I am greatly indebted to Prof Mourad HADDADI for supervising this thesis, for his support during the last four months.

Thanks are also due to Dr. Weisheng ZHAO for accepting me to do my internship at Fondamental Electronic Institute (I.E.P.) and the task of internship advisor. The chance he gave me is greatly appreciated.

I wish to express my gratitude to Professor Jacques-Olivier KLEIN my internship co-advisor. Jack's caring and supports during my internship are truly above and beyond the call of duty. He deserves more than the traditional "thanks".

I would like to thank my supervisor Professor Mourad HADDADI and my internship advisors Dr. ZHAO and Professor KLEIN for giving me the opportunity to work on this topic and for giving me the freedom and resources from which I greatly benefitted.

I also owe thanks to my best friend at IEF Dr. Djaffar CHABI, for my friend Yue ZHANG for their support and encouragement during my internship.

I wish to express my sincere gratitude to all my professors at National Polytechnic School (ENP) for their exceptional support. I owe special acknowledgements to them for all I have learned during these five years at ENP.

Thanks to all jury members for their interest and careful reading of my thesis.

Finally, I acknowledge the valuable role played by my Director and all staffs that support all time all students of ENP and allow us to achieve our studies and get our diploma as better as possible.

DEDICATION

I dedicate my thesis to my dear parents who always encourage me to do my best and support me either in difficult and best moments, shared my joys and my sorrows.

To my dear grandparents who always care and ask after me.

To my dear sisters.

To all my family.

To all my friends and my colleagues.

CONTENTS

ABBREVIATIONS

Abbreviations

A

A-FTJ: Asymmetric Ferroelectric Tunnel Junction.

C

CMOS: complementary metal-oxide-semiconductor.

CVD: Chemical Vapour Deposition.

D

DOS: Density of States.

DRAM: Dynamic Random Access Memory.

F

FeRAM: Ferroelectric Random Access Memory.

FIMS: Field Induced Magnetic Switching.

FSM: Finite State Machine.

FTB: Ferroelectric Tunnel Barriers.

FTJ: Ferroelectric Tunnel Junction.

G

GER: Giant Electroresistance.

GMR: Giant Magnetoresistance.

M

MBE: Molecular Beam Epitaxy.

MFTJ: Multi-ferroic Tunnel Junctions.

MRAM: Magnetic Random Access Memory.

MTJ: Magnetic Tunnel Junction.

P

PDF: Probability Density Function.

R

RAM: Random Access Memory.

S

SET: Single Electron Tunnelling.

S-FTJ: Symmetric Ferroelectric Tunnel Junction.

SOC: Spin Orbit Coupling.

SQID: Superconducting Quantum Interference Device.

SRAM: Static Random Access Memory.

STT: Spin Transfer Torque.

T

TAS: Thermally Assisted Switching.

TER: Tunnel electroresistance.

TMR: Tunnel Magnetoresistance.

V

VSM: Vibrating-Sample Magnetometer.

CHAPTER 1: GENERAL INTRODUCTION

Chapter 1: General introduction

1. Introduction

"The advent of semiconductor technology has impacted our daily lives since the 1970s. Silicon CMOS (complementary metal-oxide-semiconductor) devices are practically ubiquitous, and by the year 2000, the value of the semiconductor industry exceeded that of the automobile one. On the other hand, the magnetic industry remains much smaller than the semiconductor industry. Engineering schools of universities rarely cover any courses in this discipline. Nonetheless, a tiny magnetic recording device is in the hard disk of every computer. Like CMOS devices, magnetic recording technology is being scaled down more and more.

A Magnetic Random Access Memory (MRAM) chip is built by integrating magnetic tunnel junctions (MTJs) devices onto the silicon CMOS circuits. The research activity of MTJs in academia and industry, both hard disk and semiconductor, has been very active since it first showed signs of technology implication in the mid of 1990s. That effort led to the mass production of the MTJ recording head in hard disk in 2006. In the same year, the semiconductor industry announced the first successful introduction of an MTJ memory product. The viability of MTJ technology is proven. It is expected that research activities will develop further, which will increase cooperation between these two research communities." [1]

MTJ is a spintronic device and spintronic devices exploiting the spin of the electron [2-11] are prepared to revolutionise the electronics industry. The motto of MTJs is faster memory and lower power consumption at low electron density. "The late 20th century has been considered as an era of microelectronics.

However, the avalanche growth of microelectronics is a major threat to Moore's law and spintronics may be a solution for it. From the first transistor to the signally powerful microprocessor in our recent computers, most electronic devices have employed circuits that express data as binary digits, or bits (1 and 0) represented by the existence or absence of electric charge. Unlike microelectronics, spintronics exploits spin (spin up ↑ and spin down ↓) of the electron to carry information between devices." [12]

The discovery of Giant Magnetoresistance (GMR) by Nobel Prize winners Albert Fert and Peter Grünberg had actually led to the birth of novel field spintronics [13]. Currently, most of the existing spintronic devices [14] are based on metallic systems such as the MTJs and single electron transistors [15]. On the other hand, a wealth of intriguing spin phenomena has been observed in nanoscale materials [16]. This triggered an extensive research effort on spin transport in nanoscale MTJs and other interesting phenomena were realised. One of the most important phenomena is Tunnel Magnetoresistance (TMR) of the MTJs. An MTJ is composed of two ferromagnetic conducting layers separated by an ultra-thin insulating layer [17-22]. The TMR was first demonstrated by M. Jullière [23] Yakushiji et al. [24] experimentally demonstrated the influence of spin conduction on TMR. The enhancement and oscillation of TMR in ferromagnetic multiple junctions have been predicted by several authors [25-32].

2. Spintronic devices

The physical effects behind MTJs are described in "Spintronics", which is a discipline that exploits the spin property of electrons instead of positive and negative charges as in conventional electronics, see **Figure 1 (a)**. The data is therefore stored on the spin direction of electrons (i.e. "up" and "down"), see **Figure 1 (b)**. [33]

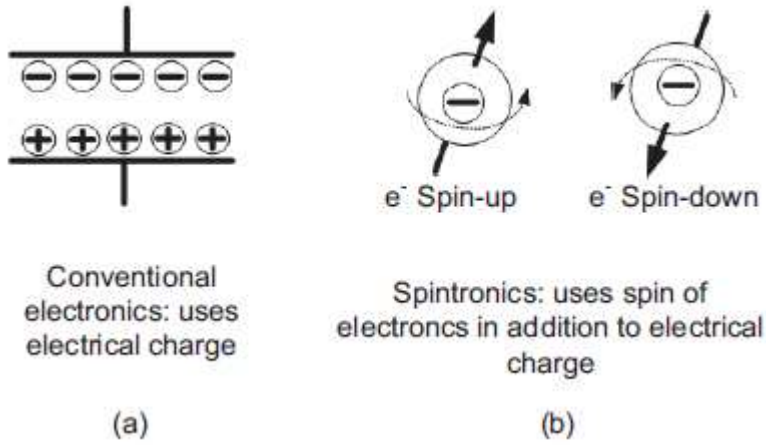

Figure 1: Comparison between principles of electronics and "Spintronics". **(a)** Conventional electronics uses only the electrical charges. **(b)** "Spintronics" exploits also the spin property of electrons. (After ref. [33])

"The working principle of a spintronic device follows the steps:

(i) Information is stored into spins as an orientation (i.e. up or down).

(ii) Spin information is carried by mobile electrons along a path or wire.

(iii) The information is then read at a final point.

Figure 2 shows the schematic representation of a spintronic device. The spin orientation of conduction electrons will exist for several nanoseconds making them useful in electronic circuit and chip design.

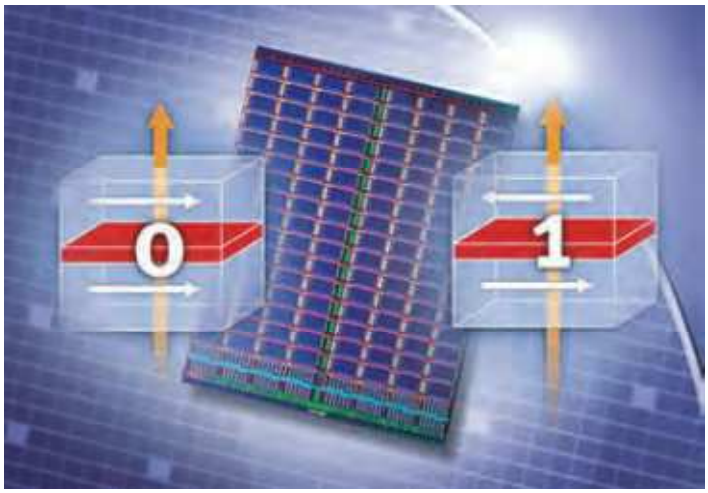

Figure 2: Schematic representation of spintronic device. (After ref. [12])

The most basic method of creating a spin-polarized current is to transport current through a ferromagnetic material and to transmit the electron spin carrying the information to the receiver point. Spin current is therefore an important tool to detect spin in spintronic devices. The important avenues for the development of spintronics devices are:

(i) Fabrication of nanoscale nanostructures including novel magnetic materials, thin films, hybrid structures, and functional materials.

(ii) Research on spin effect (spin injection, and spin transport and detection).

(iii) Demonstration of spintronic devices including giant magnetoresistance (GMR) and tunnel magnetoresistance (TMR) devices in magnetic tunnel junctions (MTJs)

(iv) Study of Single Electron Tunnelling (SET) in MTJs." [12]

"However, recent interest in the concept of ferroelectric tunnelling junctions (FTJs) using ferroelectric tunnel barriers (FTBs) begins to expand for reasons of both scientific curiosity and prospects of practical applications." [34]

"FTJs have been extensively investigated from both experimental and theoretical aspects; this laid the basis for the research on the multiferroic tunnel junctions (MFTJs)." [35]

Actually, the purpose of my internship is to investigate more about MFTJs, modelling an MFTJ and a hybrid CMOS/MFTJ circuit on *Cadence virtuoso.*

In this thesis, we will first try to understand the general functioning of spintronic devices. After, we will learn more about MTJs, FTJs, MFTJs and why these devices could bring major advantages standing then as the most promising storage technologies.

References

[1] DENNY, D. Tang, and Lee Yuan-Jen. *Magnetic Memory: Fundamentals and Technology*. 1st ed. Cambridge University Press, 2010.

[2] Y. Oshima, T.Takenobu, K. Yanagi, Y. Miyata, H. Kataura, K. Hata, Y. Iwasa, and H. Nojiri, Phys. Rev.Lett. 104, 016803 (2010).

[3] B.W. Alphenaar, K. Tsukagoshi, and M. Wagner, Physica E 10, 499 (2001).

[4] S. L.-Mei, G.Wei, C. S.-Xun, and Z. J.-Cang, Chin. Phys. Lett. 9, 3397 (2008).

[5] S.Roche, and R.Saito, Phys. Rev.Lett. 87, 246803 (2001).

[6] X. Hoffer, C. Klinke, J.-M. Bonard, L. Gravier, and J.-E.Wegrowe, Europhys. Lett. 67, 103 (2004).

[7] G. T. Kim, E. S. Choi, D. C. Kim, D. S. Suh, Y. W. Park, K. Liu, G. Duesberg, and S. Roth, Phys. Rev. B 58, 16064 (1998).

[8] F. A. Zwanenburg, D. W. van der Mast, H. B. Heersche, E. P. A. M. Bakkers, and L. P. Kouwenhoven, Nano Lett. 9, 2704 (2009).

[9] S.Krompiewskia, Acta Physica Polonica A, Proceedings of the European Conference Physics of Magnetism, (2008) June 24-27, Poznan, Poland.

[10] A. Bachtold, C. Strunk, J.-P. Salvetat, J.-M.Bonard, L. Forro, T. Nussbaumer, and C. Schonenberger, Nature, 397, 673 (1999).

[11] A. Bachtold, M. Henny, C. Terrier, C. Strunk, C. Schönenberger, J.-P. Salvetat, J.-M. Bonard, and L. Forró, Appl. Phys. Lett.73, 274 (1998).

[12] *InTech Carbon Nanotube Based Thin Films Synthesis and Properties Pdf Free Ebook Download*, n.d. http://ebookbrowse.com/intech-carbon-nanotube-based-thin-films-synthesis-and-properties-pdf-d257366273.

[13] P. Baláž, Editor *Mechanochemistry in nanoscience and minerals engineering*, Springer, Berlin Heidelberg (2008).

[14] G. Baumgartner, M. Carrard, L. Zuppiroli, W. Bacsa, Walt A. de Heer, and L. Forró, Phys. Rev. B 55, 6704 (1997).

[15] X. Lou, C. Adelmann, S A.Crooker, E S. Garlid, J. Zhang, K. S.M. Reddy, S. D. Flexner, C. J. Palmstrøm, and P. A. Crowell, Nat. Phys. 3, 197 (2007).

[16] B. Zhao, I. Mönch, H. Vinzelberg, T. Mühl, and C. M. Schneider, Appl. Phys. Lett. 80, 3144 (2002).

[17] R.P. Hunt, IEEE Trans. Mag. 7, 150, (1971).

[18] M. N. Baibich, J. M. Broto, A. Fert, F. N. V. Dau, F. Petroff, P. Etienne, G. Creuzet, A. Friederich, and J. Chazelas, Phys. Rev. Lett. 61, 2472 (1988).

[19] H. Sato, P.A. Schroeder, J. Slaughter, W.P. P. Jr., and W. A.-Razzaq, Superlatt. Microstruct. 4, 45 (1988).

[20] T. Miyazaki, and N. Tezuka, J. Magn. Magn. Mater.139, 231 (1995).

[21] Y. M. Lee, J. Hayakawa, S. Ikeda, F. Matsukura, and H. Ohno, Appl. Phys. Lett. 90, 212507 (2007).

[22] Y. M. Lee, J. Hayakawa, S. Ikeda, F. Matsukura, and H. Ohno, Appl. Phys. Lett. 89, 042506 (2006).

[23] M. Julliere, Phys. Lett. 54 225 (1975).

[24] K. Yakushiji, F. Ernult, H. Imamura, K. Yamane, S. Mitani, K. Takanashi, S. Takahashi, S. Maekawa, and H. Fujimori, Nat. Mater. 4, 57 (2005).

[25] J. Mathon and A. Umerski, Phys. Rev. B 63, 220403 (2001).

[26] G. Baumgartner, M. Carrard, L. Zuppiroli, W. Bacsa, Walt A. de Heer, and L. Forró, Phys. Rev. B 55, 6704 (1997).

[27] R. Fiederling, M. Keim, G. Reuscher, W. Ossau, G. Schmidt, A. Waag, and L. W. Molenkamp, Nature (London) 402, 787 (1999).

[28] B. Zhao, I. Mönch, H. Vinzelberg, T. Mühl, and C. M. Schneider, Appl. Phys. Lett. 80, 3144 (2002).

[29] J. Z. Cai, L. Lu1,W. J. Kong, H. W. Zhu, C. Zhang, B. Q. Wei, D. H. Wu, and F. Liu, Phys. Rev. Lett. 97, 026402 (2006).

[30] S. Krompiewski, R. Gutie´rrez, and G. Cuniberti, Phys. Rev. B 69,155423 (2004).

[31] C. Strunk, Science 306, 63 (2004).

[32] X. Hoffer, Ch. Klinke, J.-M. Bonard, L. Gravier, and J.-E. Wegrowe, Europhys. Lett. 67, 103 (2004).

[33] Lakys, Y., W.S. Zhao, J. Klein, and C. Chappert. “Hardening Techniques for MRAM-based Non-volatile Storage Cells and Logic.” In *Radiation and Its Effects on Components and Systems (RADECS), 2011 12th European Conference On*, 669 –674, 2011.

[34] Zheng, Yue, and C H Woo. “Giant Piezoelectric Resistance in Ferroelectric Tunnel Junctions.” *Nanotechnology* 20, no. 7 (February 18, 2009): 075401.

[35] Wang, Jian, Sheng Ju, and Z.Y. Li. “Bias Voltage Effect on Electron Tunneling Across a Junction with a Ferroelectric–ferromagnetic Two-phase Composite Barrier.” *Journal of Magnetism and Magnetic Materials* 324, no. 6 (March 2012): 1067–1070.

CHAPTER 2: MAGNETIC TUNNEL JUNCTIONS

Chapter 2 : Magnetic Tunnel Junctions

1. Introduction

A magnetic tunnel junction (MTJ) can be considered as a spintronic device since it is composed of two ferromagnetic materials, such as nickel, cobalt or iron, separated by an ultrathin layer of insulator with a thickness of the order of nanometre ($10^{-9}m$). It exhibits two resistances, low (R_p) or high (R_{ap}) depending on the relative direction of ferromagnet magnetizations, parallel (P) or anti-parallel (AP), respectively. The insulating layer is so thin that electrons can tunnel through the barrier if a bias voltage is applied between the two metal electrodes. The schematic of a magnetic tunnel junction (MTJ) stack is illustrated in **Figure 1**. In MTJs the tunnelling current depends on the relative orientation of magnetizations of the two ferromagnetic layers, which can be changed by an applied magnetic field. This phenomenon is called tunnel magnetoresistance (TMR).

An important factor in TMR is the interaction between the electron spin (S) and angular momentum (L) that is, spin orbit coupling (SOC). The SOC deforms the electron shell as the direction of the magnetization rotates.

This deformation also changes the amount of scattering undergone by the conduction electrons when traversing the lattice. There will be minimum resistance if the magnetizations are in parallel orientation and it will be max with opposite orientations (**Figure 2**). Therefore, such kind of junction can be easily switched between two states of electrical resistance, one with low and one with very high resistance.

A Schematic description of tunnelling magnetoresistance effect in a magnetic tunnel junction is shown in **Figure 3** [1].

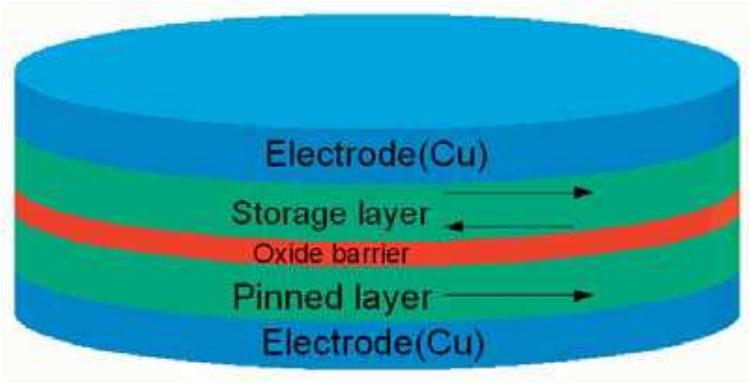

Figure 1: Magnetic tunnel junction stack. (After ref. [2])

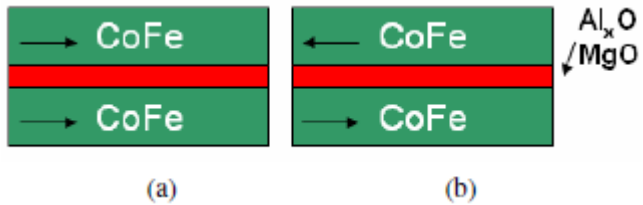

Figure 2: (a) Low resistance MTJ. **(b)** High resistance MTJ. (After ref. [3])

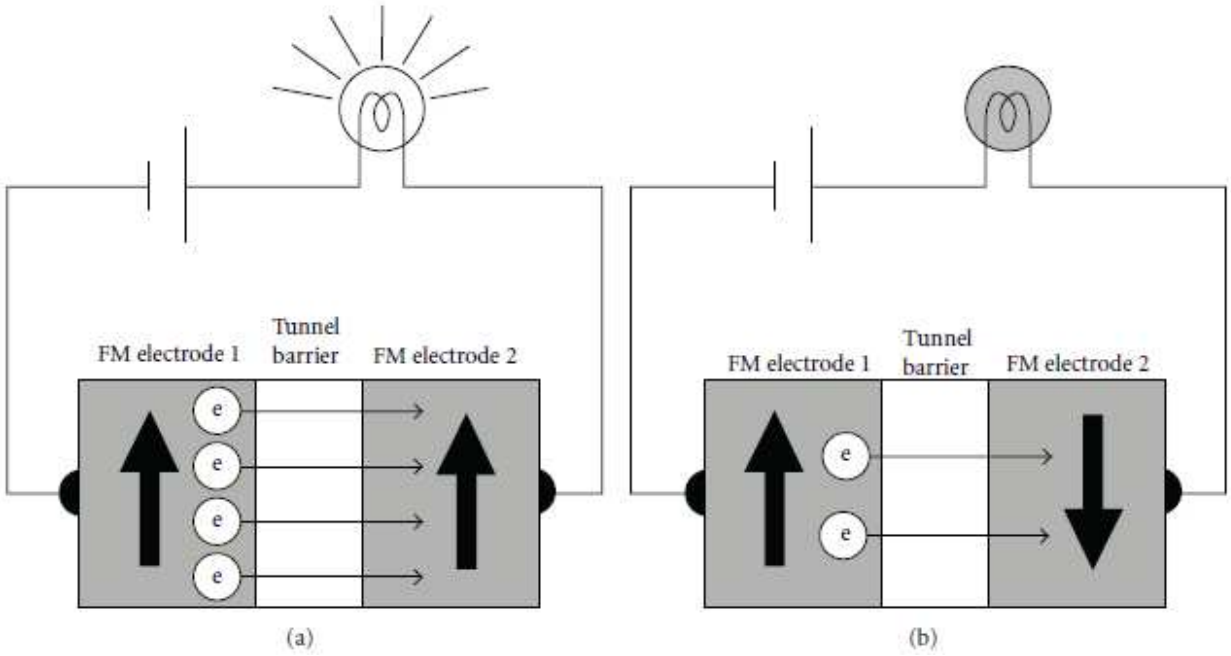

Figure 3: Schematic description of tunnelling magnetoresistance effect in a magnetic tunnel junction. Spins in the two electrodes are aligned **(a)** parallel. **(b)** Anti-parallel. (After ref. [4])

2. Fabrication of MTJs

"The fabrication of MTJs with high TMR ratios is crucial in developing spintronic devices. With the advance of nanotechnology, there are various methods to deposit MTJs, such as molecular beam epitaxy (MBE), magnetron sputtering, electron beam evaporation and chemical vapour deposition (CVD), and so on. In detail, the MTJ's main components are ferromagnetic (FM) layers and insulator layer. The FM layers can be fabricated by sputter deposition (magnetron sputtering and ion beam deposition). The fabrication issue is the magnetic alignment and thickness (deposition rates should be in the Angstrom-per-second range).

The best way of fabricating insulating layer is still under research. Some of the proven materials are Al_2O_3 tunnel barriers made by depositing a metallic aluminium layer in the range of 5-15 Å thickness. In addition, ion beam oxidation, glow discharge, plasma, atomic-oxygen exposure and ultraviolet-stimulated oxygen exposure are also alternate ways of insulator deposition. Since the first report on TMR by Julliere [5], many studies have been performed to explore this property, especially on Al_2O_3insulating layers. The necessity of controlling the magnetic properties of the magnetic layers introduces special requirements on the deposition process.

The maintaining of inherent magnetic anisotropy is crucial in the deposition process. This can be set by applying magnetic field during deposition. The thickness and uniformity of the material, the coercivity, magnetorestriction, all are important in controlling the magnetic anisotropy."[1]

There are some theoretical predictions stating the MTJs with maximum TMR ratios could be fabricated by the epitaxial growth of ferromagnetic-non ferromagnetic-ferromagnetic nanoscale sandwich structure, Fe/MgO/Fe and Fe/MgO/FeCo [6, 7]. The high ratios resulted from the effective coupling of the

majority spin band of Fe/FeCo into MgO and MgO into Fe/FeCo. TMR ratios up to 180% and 220% were achieved in these structures [8, 9]. The literature also says MTJs can be fabricated using half-metallic ferromagnets [10] and can generate 100% spin polarization at Fermi level (E_F) due to the energy gap for one spin direction. The maximum spin polarization up to 100% is highly desirable in spintronic devices for the efficient spin injection from ferromagnetic electrodes into the non-ferromagnetic spacer and for the development of current induced magnetization switching in MTJs. Other MTJs with half-metallic ferromagnets which have shown higher TMR at room temperature are cobalt based alloy thin films including $Co_2Cr_{1-x}Fe_xAl$, Co_2MnSi or $CoMnAl$. In addition to MgO tunnel barrier, aluminium oxide also been used as tunnel barrier with ferromagnetic electrodes $Co_2Cr_{0.6}Fe_{0.4}Al$ and Co_2MnSi. The advantage of these alloys is the high Curie temperature above room temperature. N. Tezuka et al have developed a MTJ of $Co_2FeAl_{0.5}Si_{0.5}$ electrodes and a MgO barrier fabricated by MBE and observed that their device had a TMR ratio of 386% at approximately 300K and 832% at 9K [11].

3. TMR in MTJs

An MTJ is a vertical stack, composed of three layers (**Figure 1**): an oxide tunnel barrier and two ferromagnetic materials (e.g. Co_2Fe) based layers [2]. A magnetoresistive effect named tunnel magnetoresistance (TMR), leading to different resistance values when the two ferromagnetic layers are in the same or opposite magnetization directions, was predicted in the stack by Julliere in 1975 [5] and observed by Moodera et al. [12] and Miyazaki and Tezuka [13] in 1995. Therefore, an MTJ stack can be used as a non-volatile memory cell if the magnetization is fixed in the pinned layer and can be changed in the storage layer [2]. The MTJ resistance is lower in the parallel (P) state where the free layer magnetization is aligned in the same direction of the fixed layer

magnetization than in the anti-parallel (AP) state where the free layer magnetization is aligned opposite to the fixed layer magnetization. Therefore, the magnetization state of the MTJ is used to store data, bit "0" or bit "1," which is detected as different resistance, (R_p) or (R_{ap}), respectively [14].

Conventional MTJs with amorphous aluminium oxide tunnel barrier (Al_xO_y) exhibit a TMR ratio up to 70% [15], which prevents efficient sensing by a CMOS circuit [16]. With modern MgO tunnel barriers, TMR ratios have been observed recently up to 500% [17]. Such a TMR ratio improves significantly the sensing performances, leads to smaller CMOS circuit and to an enhancement of the stability and accuracy of their outputs [2].

3.1. Theory of TMR

The TMR effect in MTJs can be derived using Julliere's model [5, 18-20]. According to this model the magnetoresistance is expressed:

$$TMR = \frac{R_{ap} - R_p}{R_p} = \frac{2 * P^2}{1 - P^2} \qquad (1)$$

Where R_p *and* R_{ap} are the resistance in parallel and antiparallel magnetic configuration, respectively and *P* is the spin polarization. The Differential TMR can be re-written as:

$$TMR = \frac{\left(\frac{dI}{dV_{ap}}\right)^{-1} - \left(\frac{dI}{dV_p}\right)^{-1}}{\left(\frac{dI}{dV_p}\right)^{-1}} \qquad (2)$$

According to Wiesendanger [21] the derivative of an *I-V* curve the differential conductivity is expressed as:

$$\frac{dI}{dV} = \left(\frac{2 * \pi * e^2}{\bar{h}}\right) * |t^2| * D_1 * E_F * D_2 * (E_F + eV) \qquad (3)$$

Where $|t^2|$ is the tunnel probability, D_1 and D_2 are the density of states (DOS) of the two electrodes, E_F is the Fermi energy, and V is the bias voltage applied to the electrode at low temperature.

Parameter	Description	Default Value
e	Elementary charge.	$1.602*10^{-19}$ C
$\bar{h}$	Reduced Planck constant = $h/2\pi$	$1.054*10^{-24}$ J.s
D_1	Density of state of the Electrode 1.	
D_2	Density of state of the Electrode 1.	
E_F	The Fermi energy.	
Variable	Description	Default Value
$\|t^2\|$	The tunnel Probability.	
V	Bias voltage (applied voltage).	

3.2. Characterization

It is well known that the TMR is highly sensitive to the structural and chemical nature of the material. The characterization techniques such as electrical conductivity, magnetoresistance and tunnelling microscopy can give detailed information on MTJs properties. The knowledge on magnetic property of the ferromagnetic electrodes is crucial in development of MTJ devices. The superconducting quantum interference device (SQID) is the most sensitive magnetic field equipment to measure the magnetic property. It has enough sensitivity to measure the magnetic fields in nano-scale ferromagnets. The magnetization of the material can also be measured by vibrating-sample magnetometer (VSM) technique. VSM is based on Faraday's law which implies that an electro-magnetic field will be generated in a coil when flux changes in the coil. TMR also can be measured using the four probe method by sweeping the magnetic field. Scanning tunnelling spectroscopy (STS)/scanning tunnelling microscopy (STM) is another technique which can give precise TMR measurements [1].

4. Spin current in MTJs

In the view of rapid progress in the fabrication of nanoscale MTJs, spin is a subject of great interest. Spin is a purely quantum mechanical quantity which provides an extra degree of freedom for the electron to interact with a magnetic field. In 1922, Stern and Gerlach demonstrated the most direct experimental evidence of the existence and of the quantized nature of the electron spin. The first experimental evidence of spin dependent tunnelling was reported by Jullerie [5] in 1975. Later, Berger proposed the idea that spin polarized current act on local magnetization of ferromagnets and leads to giant magnetoresistance [22].

The important property of spin is its weak interaction with the environment and with other spins, resulting in a long coherence or relaxation time, which is a very important parameter in the field of spin-transport and quantum computing. For the successful incorporation of spins into the currently existing electronics, one has to resolve issues such as efficient spin injection, spin transport, control and manipulation of spins and finally detection of spin polarized current [1].

Spintronics without magnetism is an attractive pathway for designing semiconductor spintronic devices since spin orbit coupling (SOC) enables that the spin is generated and manipulated merely by electric field. By the application of electric field, the electrons move in the lattice generating a magnetic field which acts up on the spin. The spin orbit interaction on mobile electrons was proved theoretically many decades ago. However, the practical harnessing of this concept is still at an early stage [1].

4.1. Spin transport

The influence of spin transfer in MTJs can be observed by measuring resistive loops as a measure of external applied field and applied voltage. By sweeping the magnetic and electrical field, one can observe sharp drop in resistance which

is attributed to the switching from parallel to anti-parallel and vice versa. The drop of resistance is associated with the TMR. One of the factors that affect drop of resistance and TMR is DOS at the interface [23-27].

4.2. Spin polarization

In addition to the spin transport, spin injection and spin polarization are also important factors in governing TMR. The spin polarization is a result of a subtle cancellation between two spin channels and is greatly influenced by the atomic, electronic and magnetic structures of the system. While the fundamentals of electron tunnelling are well understood, the quantitative theoretical description is lacking in real systems due to limitations in fabrication. Sophisticated and stable nanofabrication method will solve the problem of interface in MTJs [1]. However, to build up on experimental findings, it is also essential to develop an accurate model of the spin polarization and transport of spin current through the ferromagnetic/non-ferromagnetic interface and finally into vacuum which is highly sensitive to the chemical and material details of the device. In this context, Density functional theories [28] of MTJ system that can produce spin polarization effects in the Fermi Energy (E_F) are important.

5. MTJ writing methods

The MTJ switching methods are one of the most important research fields because they can influence directly the power, speed and area performance of hybrid MTJ/CMOS circuits [29].

Several MTJ writing (state switching) approaches exist:

5.1. Field Induced Magnetic Switching (FIMS)

It has been the writing approach adopted in the first generations of MRAMs. The FIMS method allows the switching of the MTJ state by applying an exterior magnetic field. It is the writing method of marketed MRAMs till now.

As we can see in **Figure 4**, we use two currents I_b and $I_w$which create a permanent magnetic field to switch the spins orientation in the free layer of the MTJ.

The anti-ferromagnetic layer 1 (AF1) with à high blocking temperature T_{b1} (~300°) is added to prevent the commutation of the pinned layer.

The principal inconvenient of this method is the high energy consumption due to the high switching currents I_b and I_w (~20 mA) [30].

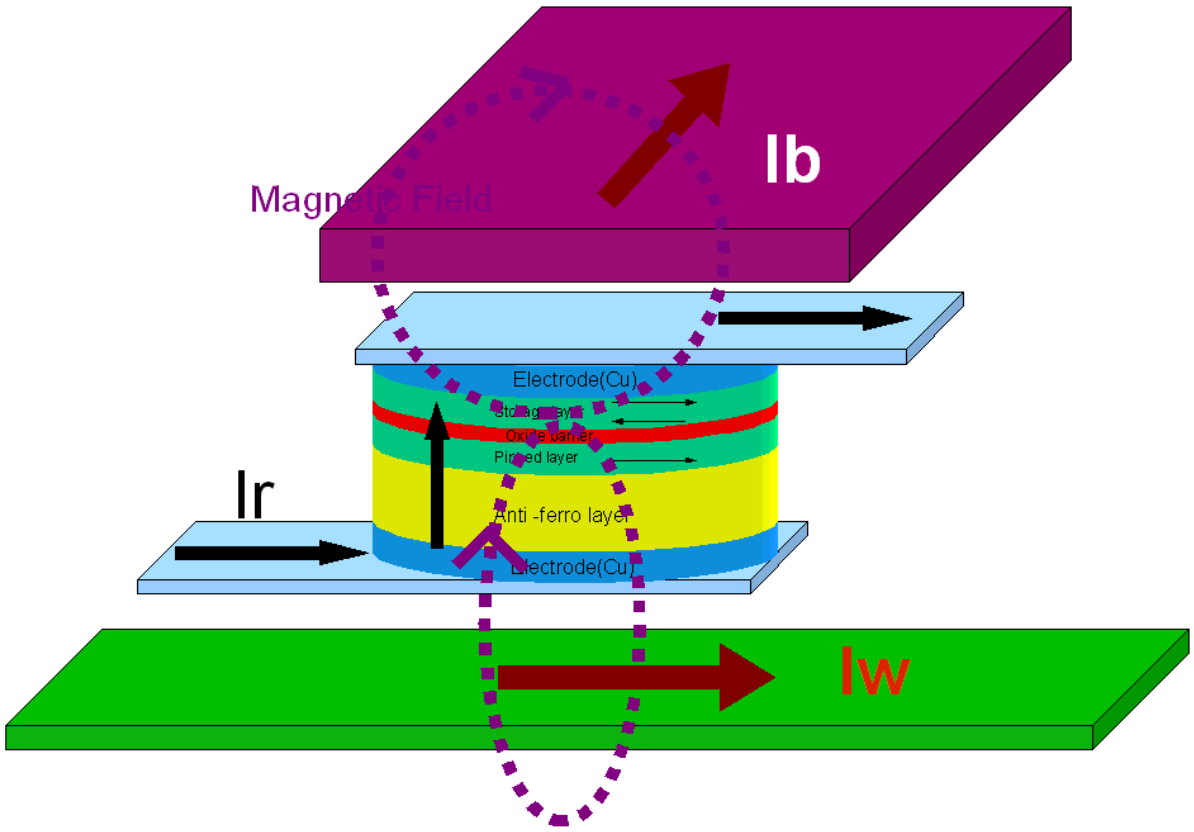

Figure 4: Structure of FIMS writing approach. (After ref [30])

5.2. Thermally assisted Switching (TAS)

This approach represents the second generation of based MTJ memories (MRAMs).

We can see in the **Figure 5**, two currents I_h and I_m. I_h (~100 µA) is to heat the MTJ and I_m (~4 mA) is to switch the MTJ [31].

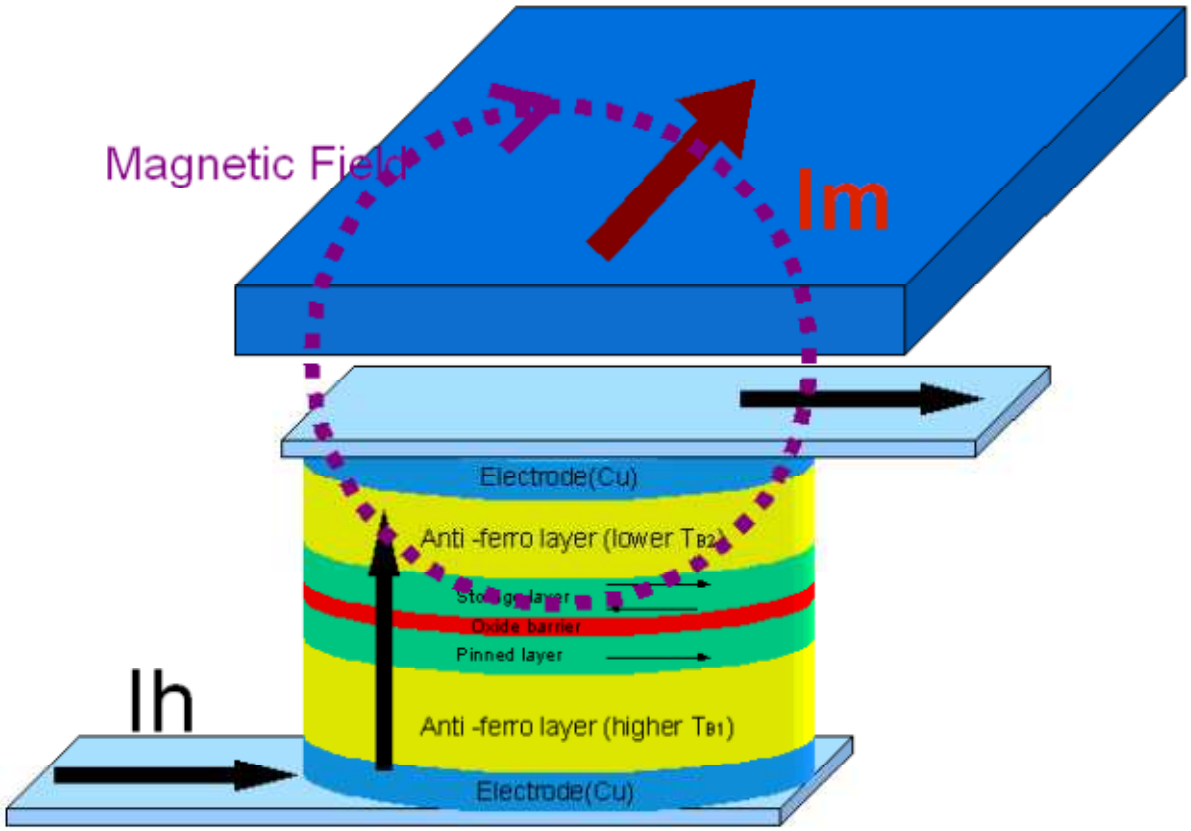

Figure 5: Structure of TAS writing approach. (After ref. [31])

Hence, the structure of the MTJ is slightly modified:

An anti-ferromagnetic layer 2 (AF2) with à low blocking temperature T_{b2} (~160°) is added top on the free layer (**Figure 6**) [31].

When the current I_h passes through the MTJ, this last one gets heated by Joule effect. After few nanoseconds, the temperature rises and overpasses T_{b2} then the switching occurs depending on the direction of the I_m current which generate a low magnetic field [31].

This writing method (TAS) presents a lower switching time and lower power consumption than the FIMS method. Nevertheless, heating and cooling durations of the MTJ slow down the switching procedure and the current remains rather high (some mA) [31].

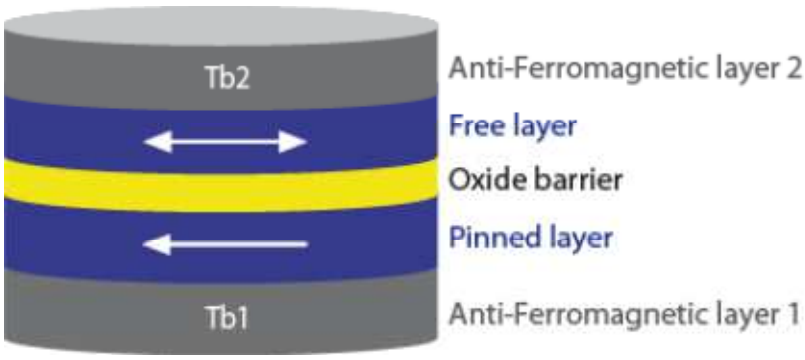

Figure 6: MTJ-TAS, an AF layer is added.

5.3. Spin-Transfer Torque (STT)

The STT switching mechanism was predicted by Slonczewski [32] in 1996 and subsequently observed by a number of research groups [33, 34].

The static behaviour is defined by the magnetization switching of the storage layer when the current density J became higher than the critical current density J_{c0} [29]. The MTJ commutates from parallel to anti-parallel or vice versa (**Figure 12**) according to its initial state and the direction of the writing current I_w.

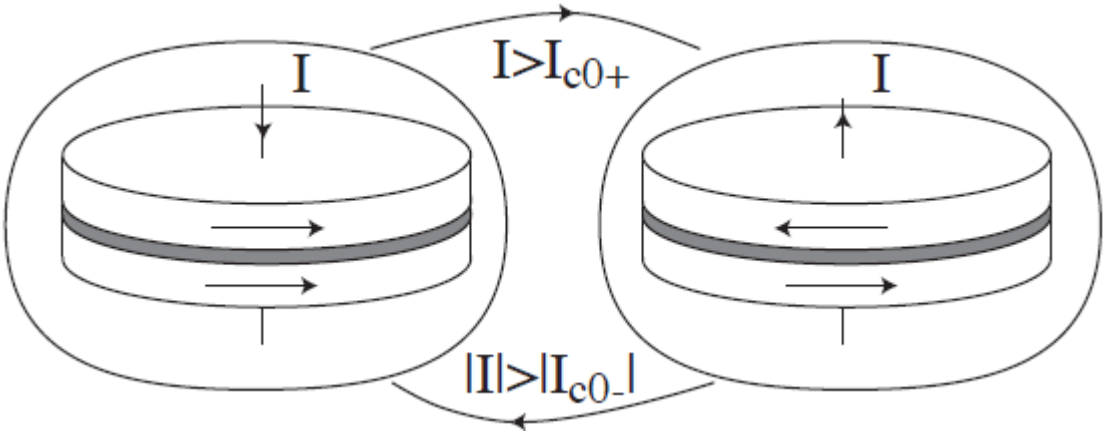

Figure 7: MTJ's state changing according to STT switching approach. (After ref. [29])

In this method, we use then only one current I_w to change the state of the MTJ (**Figure 8**). Critical current density of $8 * 10^5$ A/cm² has been found [35], leading to a writing current I_w as small as 120 µA in small size MTJs (e.g. 240*80 nm²). This last one can be generated by small MOSFETs [29].

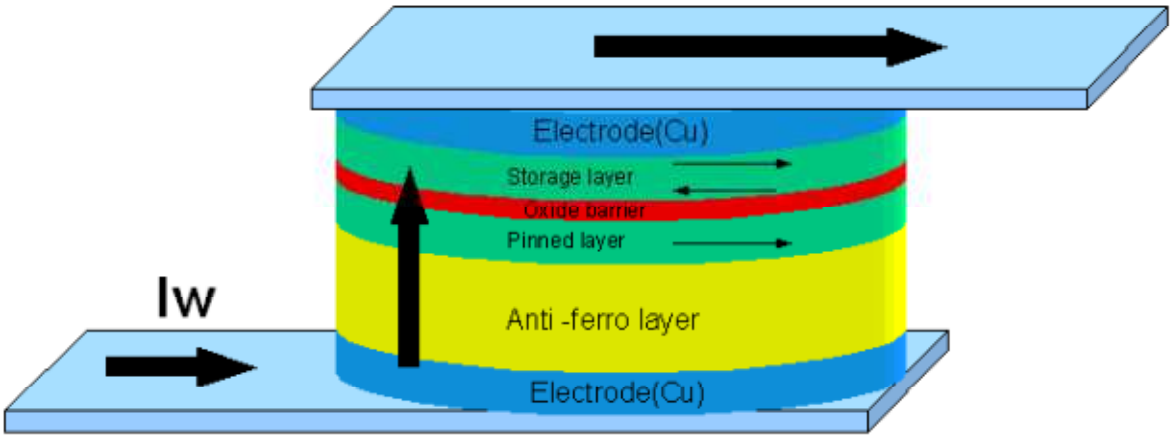

Figure 8: Structure of STT writing approach.

The low current required to switch the MTJ state in this method makes STT the most advantageous writing approach for MRAMs. However, it still presents some stability problems.

Above, I have spoken about the static behaviour of MTJs. However, the dynamic behaviour of STT-MTJ is more complex, as the switching probability interacts depends on the current pulse duration. Furthermore, this dependence follows different laws as the switching current is lower or higher than the critical current I_{c0} [29].

Four computation steps allow modelling the main dynamic behaviours of STT-MTJ:

a) Critical Current (I_{c0}) calculation: Slonczewski model

As the dynamic behaviours of STT-MTJ are different if the switching current is higher or smaller than the critical current I_{c0}, the physical model for I_{c0} calculation is firstly introduced, shown in equations (4-6) [36].

$$J_{c0} = \frac{2 * e}{\bar{h}} * \frac{\alpha * \mu_0 * M_s * d}{g} * \left(H_{ext} \pm H_{ani} \pm \frac{H_d}{2}\right) \qquad (4)$$

$$g = \left[-4 + * \left(P^{-1/2} + P^{+1/2}\right) * \left(3 + \frac{\cos(\theta)}{4}\right)\right]^{-1} \qquad (5)$$

$$I_{c0} = J_{c0} * W * L \qquad (6)$$

Parameter	Description	Default Value
e	Elementary charge.	$1.602*10^{-19}$ C
$\bar{h}$	Reduced Planck constant = *h/2π*	$1.054*10^{-24}$
α	Gilbert damping coefficient.	J.s
μ_0	Permeability in free space.	0.01
M_s	Saturation field in the storage layer.	$1.257*10^{-6}$
$\mu_0 H_{ext}$	The external magnetic induction.	H/m
$\mu_0 H_{ani}$	The in-plane uniaxial magnetic anisotropy field (negligible compared to $\mu_0 H_d$.	$-1034*10^3$ A/m -1.9 mT
$\mu_0 H_d$	The out-plane magnetic anisotropy induced by the demagnetization field.	1.3 T
P	The electron polarization.	0.52
Variable	Description	Default Value
d	Barrier thickness.	(1-3) nm
g	The spin polarization efficiency in a spin valve.	
W	The width of the junction.	80 nm
L	The length of the junction.	240
θ	$\theta = 0$, parallel and $\theta = \pi$, anti-parallel.	

b) STT-MTJ dynamic behaviour ($I < I_{c0}$): Néel-Brown model

When the current remains below its critical value, the switching can still occur due to thermal fluctuations. This erroneous condition may appear during read pulses when the current is not far to the critical current. The switching probability at any time during an under-critical current pulse can be calculated with the ratio between the energy barrier and the thermal fluctuation corrected by the current compared to its critical value (7-9) [29].

$$\frac{d}{dt} P_r(t) = {}^1/_{\tau_1} \qquad (7)$$

$$\tau_1 = \tau_0 * \exp\left(\frac{\Delta E}{k_B * T} * \left(1 - \frac{I}{I_{c0}}\right)\right) \qquad (8)$$

$$\Delta E = \frac{\mu_0 * M_s * V * H_c}{2} \qquad (9)$$

Parameter	Description	Default Value
k_B	Boltzman constant.	1.38*10^{-34} J/K
$1/\tau_0$	Attempt frequency.	1 GHz
$\mu_0 H_c$	The coercive field.	0.1 mT
Variable	**Description**	**Default Value**
τ_1	The switching time.	
V	The volume of the free layer.	
T	The temperature.	300 K

Equation (9) defines the probability density function (PDF) of an exponential law, leading to a switching probability described by equation (10).

$$P_r(t) = 1 - \exp(-t/\tau_1) \quad (10)$$

c) STT-MTJ dynamic behaviour ($I > I_{c0}$): Sun model

"When the switching (writing) current is higher than the critical one, the random effect becomes less important and the current pulse could be narrower (11-12) [37]. In this case the magnetization processes, then, after a time delay t_D, overcomes the hard axis and finally damps in the opposite magnetization direction. If the write pulse width is larger than t_D, the switching always occurs. On the contrary, if the pulse width is shorter than t_D, the switching does not occur. We model this behaviour with a finite state machine (FSM) to return in the previous state when the current pulse width is shorter than the mean delay τ_2 (**Figure 9**)."[29]

$$\tau_2 = \frac{1}{\alpha * \mu_0 \gamma * M_s} * \frac{I_{c0}}{I - I_{c0}} * \ln\left(\frac{\pi}{2 * \theta_0}\right) \qquad (11)$$

$$\theta_0 = \sqrt{\frac{k_B * T}{H_c * \mu_0 M_s * V}} \qquad (12)$$

Parameter	Description	Default Value
$\mu_0\gamma$		221 kHz/(A/m)
Variable	Description	Default Value
τ_2 θ_0	The delay time. The initial angle between the magnetization of the free layer and the hard axis.	$\theta_0 = 7.7°$, for T= 300 K

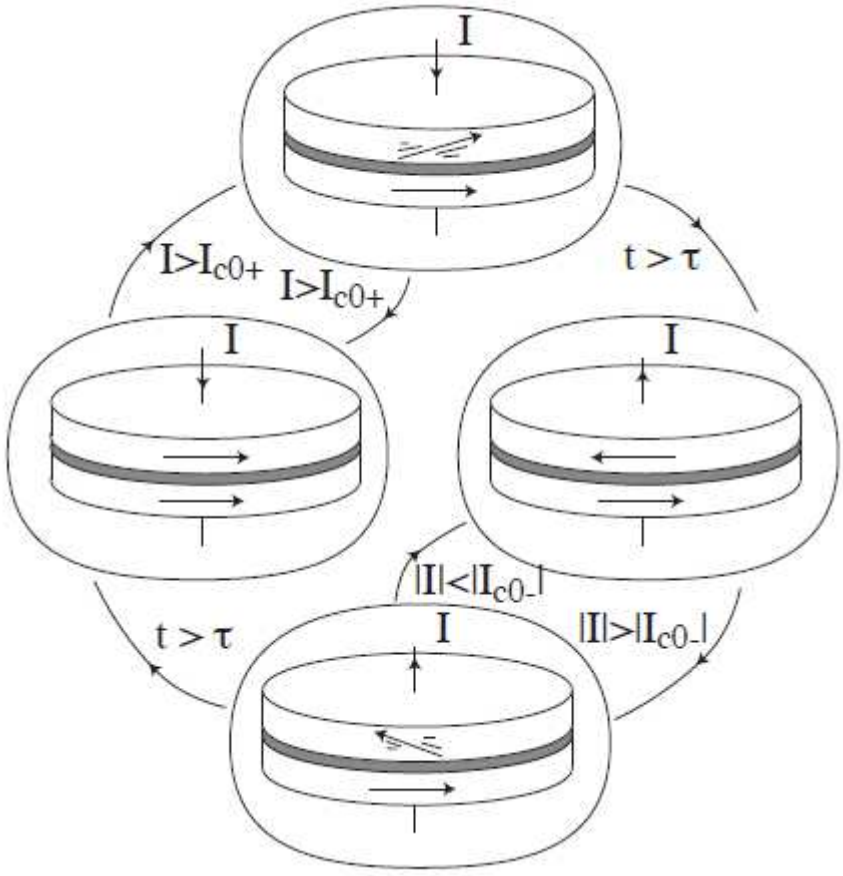

Figure 9: The insertion of intermediate states in the Finite State Machine describing the MTJ dynamic for over-critical current allows modelling the switching delay. (After ref. [29])

d) Heating and consequences in STT-MTJ

From equations (7-11), we can see that the dynamic behaviours of STT-MTJ depend highly on the thermal fluctuation and the temperature will assist the switching of STT-MTJ [38]. This effect promises the ultimate scalability for the MTJ technology. Furthermore, the temperature of STT-MTJ could be improved

simply by the current pulse; thereby the fourth calculation step takes into account the dynamic behaviours of the heating resulting from the current (13-14) [36].

$$\frac{V_{MTJ} * J}{2 * \lambda/l} = (T - T_0) + \tau_{th} * \frac{dT}{dt} \qquad (13)$$

$$\tau_{th} = \frac{C_v * e}{2 * \lambda/l} \qquad (14)$$

The dynamic of temperature follows the equation (15) during heating and (16) during cooling.

$$T_{rise} = T_0 + \frac{V_{MTJ} * I}{2 * \lambda/l} * \left\{1 - exp\left(\frac{-t}{\tau_{th}}\right)\right\} \qquad (15)$$

$$T_{cool} = T_0 + (T_{rise} - T_0) * exp\left(\frac{-(t - t_0)}{\tau_{th}}\right) \qquad (16)$$

Parameter	Description	Default Value
T_0	The room temperature.	300 K
λ	The thermal conductivity.	1.5 W/m.K
l	The thickness of the MTJ.	10 nm
C_v	The average heat capacity per unit volume	$3.47 * 10^6$ J/m³.K
Variable	Description	Default Value
V_{MTJ}	The voltage across the MTJ.	
J	The current density.	
t_0	The duration of current pulse.	
T_{rise}	The temperature of STT-MTJ after the current pulse.	
T_{cool}	The temperature of STT-MTJ after the cooling duration.	

5.4. Spin-Transfer Torque-Thermally Assisted Switching (STT-TAS)

This new switching method for MTJ nanopillars represents the best compromise between data reliability, density and power efficiency [39].

In this method, we combine the two last methods (TAS and STT). As for TAS and STT, we have to add an anti-ferromagnetic layer (AF2) and only one current is required for the MTJ switching. This current heats the tunnel junction and

when its temperature reaches the blocking temperature T_{b2} (~160°) and the current is higher than the critical current I_{c0}(~ 450 µA) [39], the MTJ switching occurs. By this hybrid writing approach, we can satisfy at the same time a good thermal stability and low energy consumption (low writing current). Furthermore, the switching time decreases (~ 6 ns) making the MTJ switching faster.

a) Temperature evaluation model

The temperature evaluation of MTJ depends on the form and duration of the switching current according to equations 17 and 18 [40, 41]. Equation 1 can be simplified to equation 19 and 20 to describe respectively the heating and cooling operations driven by a current pulse. This model allows simulating the thermally assisted mechanism of our STT-TAS approach [39].

$$\frac{V_{MTJ} * J}{2 * \lambda/thick\_b} = (T - T_R) + \tau_{th} * \frac{dT}{dt} \qquad (17)$$

$$\tau_{th} = \frac{C_v * thick\_s}{2 * \lambda/thick\_b} \qquad (18)$$

$$T_{heat} = T_R + \frac{V_{MTJ} * I}{2 * \lambda/thick\_b} * \left\{1 - exp\left(\frac{-D_{heat}}{\tau_{th}}\right)\right\} \qquad (19)$$

$$T_{cool} = T_R + (T_{heat} - T_R) * exp\left(\frac{-D_{cool}}{\tau_{th}}\right) \qquad (20)$$

Parameter	Description	Default Value
T_R	The room temperature.	300 K
λ	The thermal conductivity of the thermal barrier.	
l	The thickness of the MTJ.	
C_v	The average heat capacity per unit volume	
τ_{th}	The characteristic heating/cooling time.	
$thick\_b$	The thickness of the thermal barrier.	
$thick\_s$	The total thickness of the MTJ.	
Variable	Description	Default Value

V_{MTJ}	The voltage across the MTJ.	
J	The current density.	
D_{heat}	The heating current pulse duration.	
D_{cool}	The cooling current pulse duration.	
T_{rise}	The temperature of STT-MTJ after the current pulse.	
T_{cool}	The temperature of STT-MTJ after the cooling duration.	

Figure 10 (a) represents an equivalent electrical circuit corresponding to Equation 1 and monitoring the temperature evaluation of MTJ. Adding a multiplier (M0) and an adder (A0) allows us to observe the temperature T through the voltage node V_{temp} (i.e. 1V = 1K). The values of R_0 and C_0 are set as constant to obtain τ_{th} calculated by Equation 18 [39].

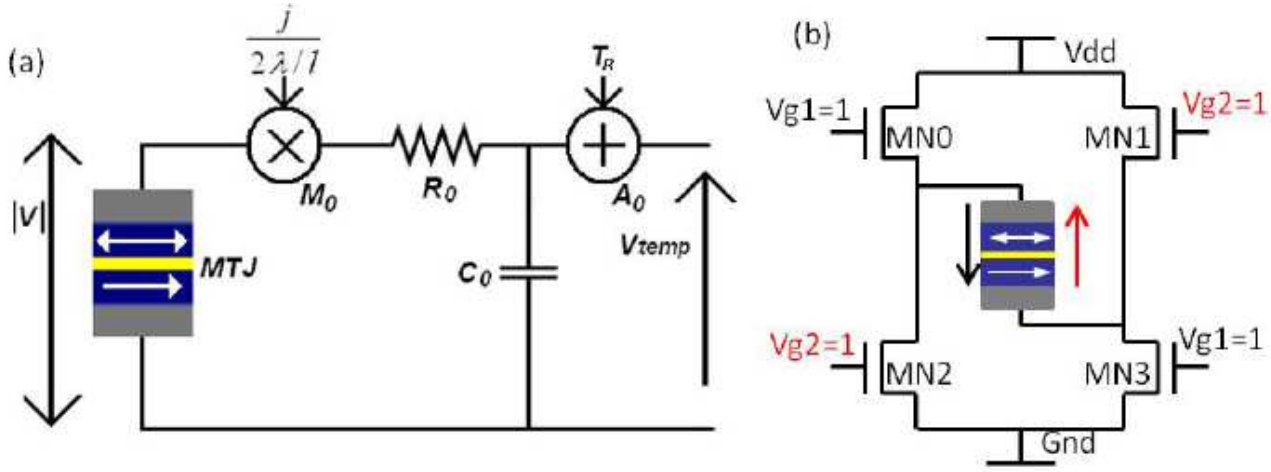

Figure 10: Circuit implementation for modelling and simulation. **(a)** Equivalent electrical RC circuit of temperature evaluation model. **(b)** MTJ switching circuit; either "V_{g1}" or "V_{g2}" is set to '1' to generate the current I_{switch}. RC, resistor/capacitor. (After ref. [39])

b) STT dynamic switching model

Equations 21 and 22 describe the STT dynamic switching; we use them to simulate the speed and power performances of hybrid MTJ/CMOS circuits [39]. Equation 22 expresses the initial angle θ_0 between the magnetization of the storage layer (free layer) and its easy axis induced by thermal fluctuations [42]. High temperature increases θ_0 and then reduces the STT switching duration D_{switch}. STT state reversal depends on switching current value I_{switch} which

should be higher than the critical current, I_{c0} [39]. With high I_{switch}, D_{switch} can be linearly reduced down [43].

$$D_{switch} = \frac{1}{\alpha * \gamma_0 * \mu_0 M_s} * \frac{I_{c0}}{I_{switch} - I_{c0}} * \ln\left(\frac{\pi}{2 * \theta_0}\right) \quad (21)$$

$$\theta_0 = \sqrt{\frac{k_B * T}{H_{ani} * \mu_0 M_s * V}} \quad (22)$$

Parameter	Description	Default Value
α	The Gilbert damping coefficient.	
γ_0	The gyromagnetic constant.	1.38*10^{-34} J/K
k_B	Boltzman constant.	1 GHz
$1/\tau_0$	Attempt frequency.	0.1 mT
$\mu_0 M_s$	The saturation field in the storage layer.	
H_{ani}	The in-plane uniaxial magnetic anisotropy field.	
Variable	Description	Default Value
D_{switch}	The switching duration.	
θ_0	The initial angle between the magnetization of the free layer and the hard axis.	$\theta_0 = 7.7°$, for T= 300 K
V	The volume of the storage layer.	
T	The temperature.	300 K

c) Compact model simulation Hybrid MTJ/CMOS circuit

"This compact model has been developed in Verilog-A language and implemented on Cadence Virtuoso CAD platform [44]. Its default parameters correspond to a MTJ nanopillar BiFe(10)/IrMn(6)/CoFeB(1)/MgO(0.85)/CoFeB (3)/PtMn(6) [39]. By using CMOS 65 nm design-kit, a simple hybrid circuit (**Figure 2 (b)**) [45] has been successfully simulated (**Figure 11**), which validates the functionalities and behaviours of this model.

The voltage pulse "V_{g1}" is activated at 40 ns and I_{switch} begins to heat the MTJ from ambient temperature. As its temperature reaches up to T_{b2} after ~ 11.22 ns, the model compares the I_{switch} (~ 463 uA) with the STT critical current I_{c0} (~ 150 uA) and switches the state of MTJ from parallel (P) to anti-parallel (AP)

state in about 6 ns according to the STT dynamic model. As "V_{g1}" is deactivated, MTJ begins to cool down to ambient temperature. The state can be reversed from AP to P by activating the control signal "V_{g2}", which generates I_{switch} (~376 μA). The I_{switch} values are asymmetric as a constant voltage supply is used in the simulation (e.g. 1V) and the resistance of MTJ changes between two states (R_p and R_{ap}) [39]. It is important to note that the voltage pulse width should be longer than D_{heat}+D_{switch} to ensure the reliable switching operation [46]." [39]

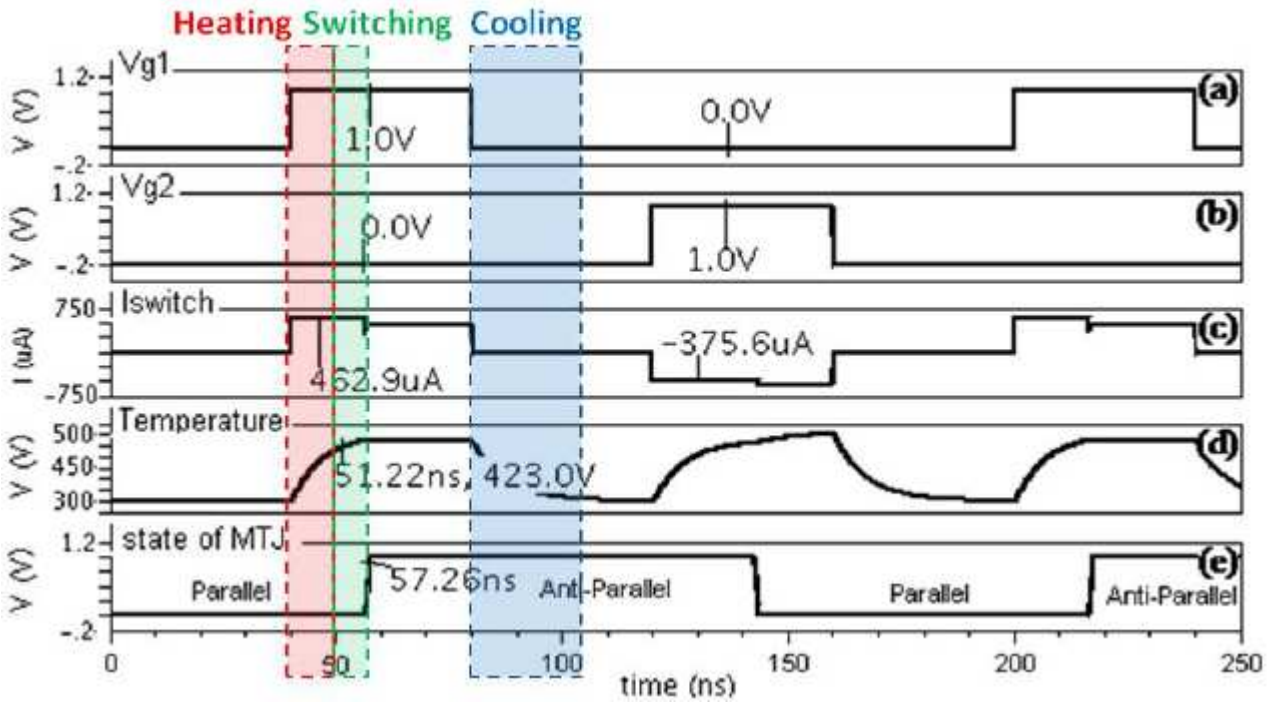

Figure 11: Transient simulation of compact model. **(a)** and **(b)** Control signals activate the circuit to generate bidirectional currents. **(c)** MTJ is switched between the P and AP. **(d)** Temperature evaluation. **(e)** The state of MTJ. P, parallel; AP, anti-parallel. (After ref. [39])

5.5. Domain wall writing

MTJ/CMOS hybrid circuits are a promising and reachable solution to eliminate logic CMOS circuit's drawbacks, specially their static energy consumption and dissipation due to leakage current within them.

However, other magnetic components and other methods to realize tiny and low power consumption logic circuits exist. One of them is Domain Wall.

In magnetism, a domain wall is a mobile interface separating two magnetic domains (**Figure 12**).

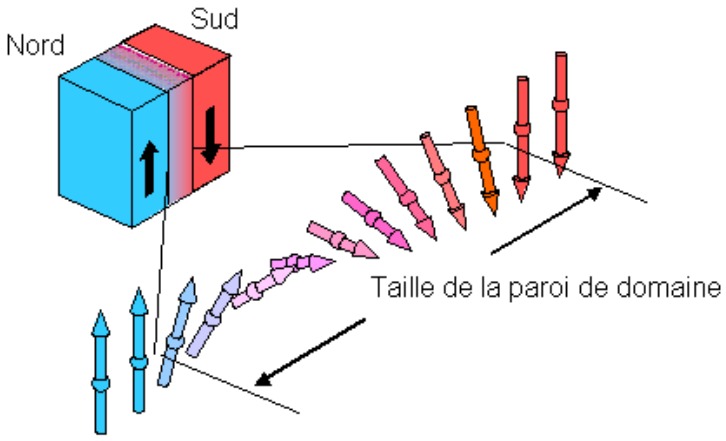

Figure 13: Domain wall.

Unlike all the writing methods discussed before, in this approach (DomainWall) the free layer does not switch but a set of layers of opposite magnetizations moves when a low current (~ 500 μA) is injected (**Figure 14** and **Figure 15**).

The high speed displacement (~ 100 m/s) of the domains allows a very small MTJ switching time (~ 2 ns).

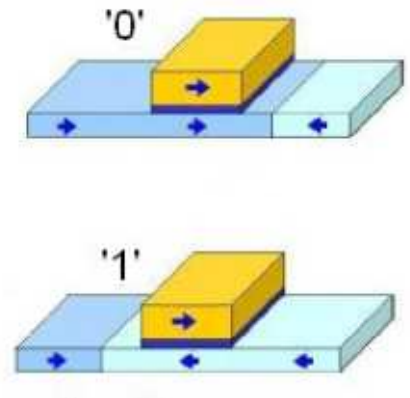

Figure 14: The walls of different magnetizations move so as to code a binary information.

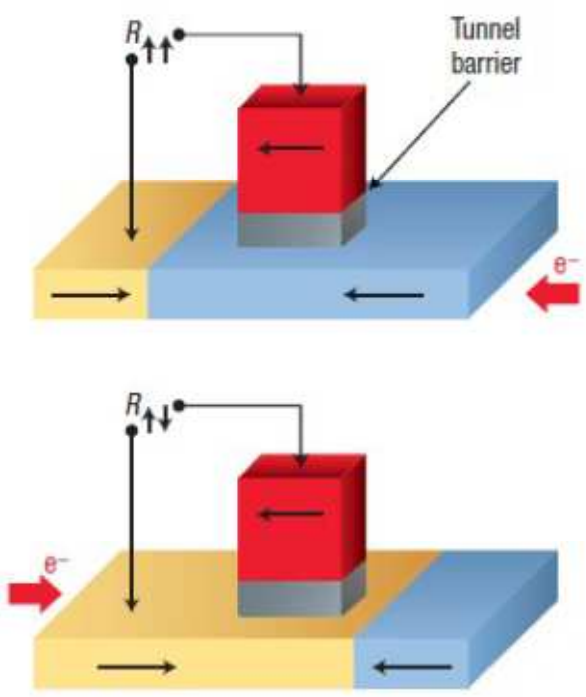

Figure 15: The walls move to the right or to the left according to the current direction.

The orientation of a moving layer can be modified when a current of ~ 250 µA order crosses it. This orientation depends on the direction of the injected current. The structure of the whole moving layers is manufactured in a way as they utilize the minimum of surface possible to guarantee a high integration density. It must also allow a correct wall trapping (**Figure 16** and **Figure 17**).

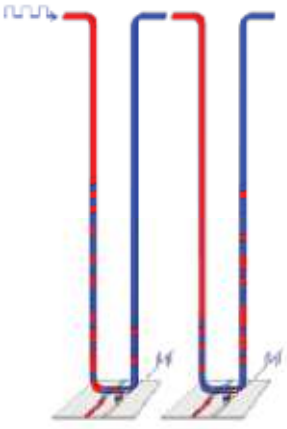

Figure 16: The vertical structure requires fewer surfaces.

Figure 17: The serpentine structure traps either side of the MTJ wall.

The domain Wall method presents several advantages like non-volatility, low manufacturing cost, low dissipation and low power consumption.

Several researches are led since 2007 to develop more this approach, notably NanoTrans group of IEF (Institut d'Electronique Fondamentale) which obtains several patents for this technology.

6. Comparison between the writing methods

The following table summarizes the different writing approaches described before:

MTJ Writing method	Area	Read/Write speed	Threshold current	Required power
FIMS	Large	High	~ 20mA	Very High
TAS	Average	Average	~ 2mA	High
STT	Small	Very high	~ 120uA	Low
STT-TAS	Small	High	~ 450uA	Average
Domain Wall	Small	Very high	~ 500uA	Average

References

[1] *InTech Carbon Nanotube Based Thin Films Synthesis and Properties Pdf Free Ebook Download*, n.d. http://ebookbrowse.com/intech-carbon-nanotube-based-thin-films-synthesis and-properties-pdf-d257366273.

[2] Zhao, Weisheng, Eric Belhaire, Claude Chappert, François Jacquet, and Pascale Mazoyer. "New Non-volatile Logic Based on spin-MTJ." *Physica Status Solidi (a)* 205, no. 6 (2008): 1373–1377.

[3] Zhao, W., E. Belhaire, Q. Mistral, C. Chapped, V. Javerliac, B. Dieny, and E. Nicolle. "Macro-model of Spin-Transfer Torque Based Magnetic Tunnel Junction Device for Hybrid Magnetic-CMOS Design." In *Behavioral Modeling and Simulation Workshop, Proceedings of the 2006 IEEE International*, 40 –43, 2006.

[4] S. Yuasa and D. D. Djayaprawira, "Giant tunnel magnetoresistance in magnetic tunnel junctions with a crystalline MgO(0 01) barrier," *Journal of Physics D*, vol. 40, no. 21, pp. R337–R354, 2007.

[5] M. Julliere, Phys. Lett. 54, 225 (1975).

[6] S. Yuasa, J. Phys. Soc. Jpn. 77,031001 (2008).

[7] E. Y. Tsymbal, O. N. Mryasov, and P. R. LeClair, J. Phys.: Condens. Matter 15, R109 (2003).

[8] C. Tiusan, F. Greullet, M. Hehn, F. Montaigne, S. Andrieu and A. Schuhl, J. Phys.: Condens. Matter 19,165201(2007).

[9] S. Ikeda, J. Hayakawa, Y. M. Lee, T. Tanikawa, F. Matsukura, and H. Ohno, J. Appl. Phys. 99, 08A907 (2006).

[10] C. Park, J.-G. Zhu, Y. Peng, D.E. Laughlin, and R. M. White, IEEE Trans. Magn. 40, 182 (2004).

[11] N. Tezuka, N. Ikeda, F. Mitsuhashi, and S. Sugimoto, Appl. Phys. Lett. 94, 162504 (2009).

[12] J. S. Moodera, L. R. Kinder, T. M. Wong, and R. Meservey, Phys. Rev. Lett. 74, 3273 (1995).

[13] T. Miyazaki and N. Tezuka, J. Magn. Magn. Mater. 139, 231 (1995).

[14] Xi, Haiwen, J. Stricklin, Hai Li, Yiran Chen, Xiaobin Wang, Yuankai Zheng, Zheng Gao, and M.X. Tang. "Spin Transfer Torque Memory With Thermal Assist Mechanism: A Case Study." *Magnetics, IEEE Transactions On* 46, no. 3 (March 2010): 860 –865.

[15] K. D. Belashchenko, J. Velev, and E. Y. Tsymbal, Phys. Rev. B 72, 140404 (2005).

[16] W. Zhao, E. Belhaire, and C. Chappert, IEEE Int. Conf. Nanotechnology, Hong Kong, China, 2007, pp. 40–43.

[17] Y. M. Lee, J. Hayakawa, S. Ikeda, F. Matsukura, and H. Ohno, Appl. Phys. Lett. 90, 212507 (2007).

[18] S. Ikeda, K. Miura, H. Yamamoto, K. Mizunuma, H. D. Gan, M. Endo, S. Kanai, J. Hayakawa, F. Matsukur and H. Ohno, Nat. Mat. 9, 721(2010).

[19] J. S. Moodera, L. R. Kinder, T. M. Wong, and R. Meservey, Phys. Rev. Lett. 74, 3273 (1995).

[20] S.S.P. Parkin, K.P. Roche, M.G. Samant, P.M. Rice, R.B. Beyers, R.E. Scheuerlein, E.J. O'Sullivan, S.L. Brown, J. Bucchigano, D.W. Abraham, Y. Lu, M. Rooks, P.L. Trouilloud, R.A. Wanner, and W.J. Gallagher, J. Appl. Phys. 85, 5828 (1999).

[21] R. Wiesendanger, Editor *Scanning Probe Microscopy and Spectroscopy*, New York: Cambridge University Press, 1994.

[22] L. Berger, J. Appl. Phys. 49, 2156 (1978).

[23] E. Y. Tsymbal, K. D. Belashchenko, J. Velev, S. S. Jaswal, M. V. Schilfgaarde, I. I. Oleynik, and D. A. Stewart, Prog. Mater. Science 52, 401 (2007).

[24] A. N. Chantis, K. D. Belashchenko, D. L. Smith, E. Y. Tsymbal, M. V. Schilfgaarde, and R. C. Albers, Phys. Rev. Lett. 99, 196603 (2007).

[25] J. D. Burton, R. F. Sabirianov, J. P. Velev, O. N. Mryasov, and E. Y. Tsymbal, Phys. Rev. B 76, 144430 (2007).

[26] H. Suzuura, and T.Ando, Physica E 6, 864 (2000).

[27] J.-G. Zhu and C. Park, Mater. Today 9, 36 (2006).

[28] R. Arras, L. Calmels, and B. Warot-Fonrose, IEEE Trans. Magn.46, 1730 (2010).

[29] Faber, L.-B., Weisheng Zhao, J.-O. Klein, T. Devolder, et C. Chappert. « Dynamic compact model of Spin-Transfer Torque based Magnetic Tunnel Junction (MTJ) ». In *Design Technology of Integrated Systems in Nanoscal Era, 2009. DTIS '09. 4th International Conference on*, 130 -135, 2009.

[30] B. N. Engel et al., "A 4-Mb toggle MRAM based on a novel bit and switching method," Magnetics, *IEEE Transactions on*, vol. 41, pp. 132--136, 2005.

[31] Chaudhuri, S., Weisheng Zhao, J.-O. Klein, C. Chappert, and P. Mazoyer. "Design of TAS-MRAM Prototype for NV Embedded Memory Applications." In *Memory Workshop (IMW), 2010 IEEE International*, 1 –4, 2010.

[32] J. C. Slonczewski, J. Magn. Magn. Mater. 59, 1 (1996).

[33] J. Z. Sun, IBM J. Res. Dev. 50, 81 (2006).

[34] J. Hayakawa, S. Ikeda, Y. Lee, R. Sasaki, T. Meguro, F. Matsukura, H. Takahashi, and H. Ohno, Jpn. J. Appl. Phys. 44, 1267 (2005).

[35-24] J.Hayakawa, S.Ikeda, Y.M.Lee, R.Sasaki, T.Meguro, F.Matsukura, H.Takahashi and H.Ohno, "Current-driven magnetization switching in CoFeB/MgO/CoFeB magnetic tunnel junctions" Japanese Journal of Applied physics, Vol.44, No.41,2005, pp. L1267-L1270.

[36] J.C.Slonczewski, J.Magn. &Magn. Mater. 159 (1996) L1.

[37] RC.Sousa, IL.Prejbeanu, D.Stanescu, B.Rodmacq, O.Redon, B.Dieny, JG.Wang and PP. Freitas, "Tunnelling hot spots and heating in magnetic tunnel junctions", Journal of Applied Physics, 95, pp.6783- 6785.

[38] B.Dieny, R.Sousa, G.Prenat, U.Ebels, "Spin-dependent phenomena and their implementaition in spintronic devices", VLSI Technology, Systmes and Applications, 2008, pp.70-71.

[39] Zhao, Weisheng, Julien Duval, Jacques-Olivier Klein, and Claude Chappert. "A Compact Model for Magnetic Tunnel Junction (MTJ) Switched by Thermally Assisted Spin Transfer Torque (TAS + STT)." *Nanoscale Research Letters* 6, no. 1 (April 28, 2011): 368.

[40] Roldan AM, Roldan JB, Reig C, Cubells-Beltran MD, Ramirez D, Cardoso S, Freitas PP: "A DC behavioral electical model for quasi-linear spin-valve devices including thermal effects for circuit simulation". Microelectron J 2011, 42:365-370.

[41] Sousa RC, Prejbeanu IL, Stanescu D, Rodmacq B, Redon O, Dieny B, Wang JG, Freitas PP: "Tunneling hot spots and heating in magnetic tunnel junctions". J Appl Phys 2004, 95:6783-6785.

[42] Koch RH, Katine JA, Sun JZ: "Time-Resolved Reversal of Spin-Transfer Switching in a Nanomagnet". Phys Rev Lett 2004, 92:088302.

[43] Devolder T, Hayakawa J, Ito K, Takahashi H, Ikeda S, Crozat P, Zerounian N, Kim JV, Chappert C, Ohno H: "Single-Shot Time-Resolved Measurements of Nanosecond-Scale Spin-Transfer Induced Switching: Stochastic Versus Deterministic Aspects". Phys Rev Lett 2008, 100:057206.

[44] Virtuoso Spectre Circuit Simulator User Guide: 2006.

[45] Zhao WS, Belhaire E, Chappert C, Mazoyer P: "Power and Area Optimization for Run-Time Reconfiguration System On Programmable Chip Based on Magnetic Random Access memory". IEEE Trans Magn 2009, 45:776-780.

[46] Prejbeanu IL, Kerekes M, Sousa RC, Sibuet H, Redon O, Dieny B, Nozière JP: "Thermally assisted MRAM". J Phys Condensed Matter 2007, 19:165218.

CHAPTER 3: APPLICATION OF MTJs IN MAGNETIC MEMORIES

Chapter 3: Application of MTJs in Magnetic Memories

1. Application of MTJs

With wider knowledge on how to manipulate spins [1], we can build more state of the art spintronic devices with extraordinary properties. Extended research into application possibilities of any spintronic effects is therefore crucial to realise more advanced spintronic devices. These devices made huge impact on computer technology by enabling higher storage of information in hard drives and faster reading of data in random access memories (RAMs).

The first successful application of MTJ was demonstrated in computer read head technology with Al_2O_3 barrier and MgO barrier MTJ. The magnetic recording density in hard disk drive increased (300-600 Gbit/Inch^2) considerably in these devices [2-5].

Magnetic random access memory (MRAM) is one of the most promising memory technologies, which features non-volatility, high reading speed, large retention time up to 10 years and it allows also more than thousand of billion (10^{12}) re-programming cycles [6]. Of course, MTJ is the elementary storage device for MRAMs; hence the performances of these last ones depend significantly on those of MTJs. The reading performance of MRAM has been significantly enhanced but its writing performance still dominates the power consumption and the circuit surface [6].

It has been claimed that MRAM can exceed the speed of SRAM (static RAM), density of DRAM (Dynamic RAM) and non-volatility of flash memory. In addition, the nano-dimension device has low power consumption and less

heating. MRAM is an upgrade version of SRAM and DRAM where data is stored using spin instead of electrical charges. It overcomes one of the disadvantages of the conventional RAM, the loss of information by power failure. Leading companies like IBM, Motorola, and Honeywell started the MRAM research in 1995 and they were supported by United States Defence Advanced Research Projects Agency (DARPA). **Figure 1** shows the images of MRAM used by leading companies like Thoshiba, IBM and Motorola.

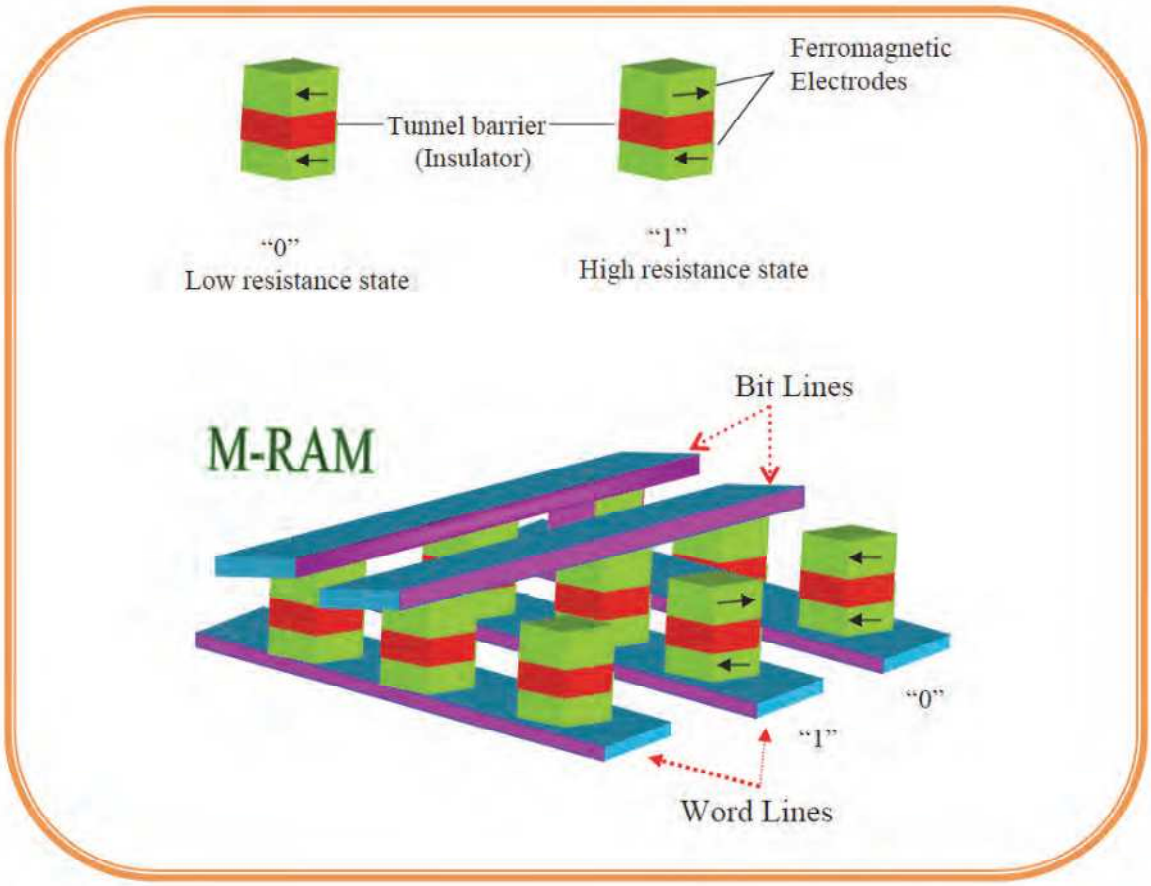

Figure 1: MRAM memory cells composed of a magnetic tunnel junction (MTJ). States "0" and "1" in the cells correspond to the parallel and anti-parallel states. (After ref. [7])

2. Hybrid MTJ/CMOS logic design

2.1. Sensing circuit: sense amplifier

MTJ device presents the resistance property compatible with CMOS transistors, which enables the sensing of the MTJ's configuration with CMOS amplifier

circuits. **Figure 2** represents the simplified sensing circuits for MRAMs [8], where there use an MTJ with midpoint value between the maximum and minimum resistance as reference to compare the MTJs in the array. This system allows the MRAMs to be realized in high density and high reading speed; however it is not suitable for logic applications, because in most of logic components as register or Flip-Flop, the memorization cells are distributed in the whole chip, local sensing is then required for those logic components.

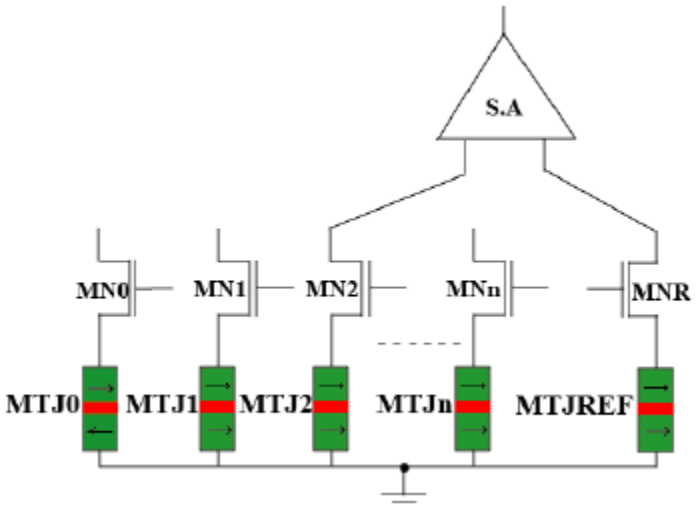

Figure 2: Schematic of Amplification circuits for MRAM.

SRAM based 5Transistors sense amplifier and a two-MTJ complementary structure (see **Figure 3**) [9] is used in our hybrid MTJ/CMOS logic design, which works in low power, high speed and with low surface. The two MTJs are configured in a complementary mode to present one logic bit; if one MTJ has a high resistance value whereas the other has a low resistance value.

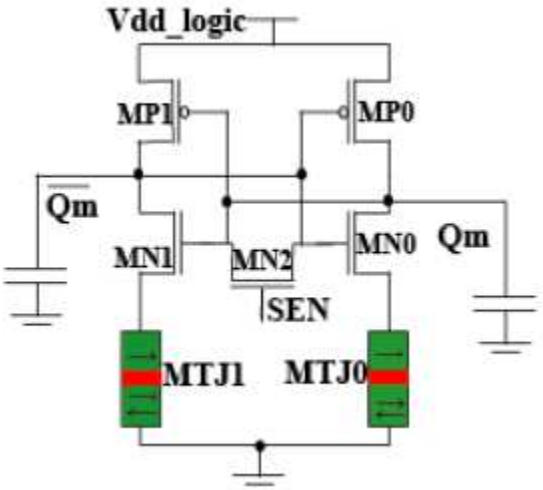

Figure 3: Schematic of SRAM based Sense Amplifier.

The information bit is available as the difference of resistances and it is transferred to two-MTJ complementary structure during the sense phase, which begins by briefly turning on the switch MN2 to place the amplifier in a metastable state.

As MTJ1 with anti-parallel configuration and MTJ0 with parallel configuration present high resistance and low resistance respectively (**Figure 4 (a)**), the currents passing through MP0-MP1, MN2 and MTJ0-MTJ1 show the relationship as shown in equations 1 and 2, the voltage difference between $Q_m$and $\overline{Q_m}$ is generated by the current I_0 passing through MN2.

When "SEN" is changing from '1' to '0' and MN2 is turning off, I_0will disappear immediately, as a result, I_1 will then be increased and I_4 will be decreased at the same time, however the charge in the two capacitances is still at the last state, electrons from V_{dd_logic} (1.2 V for STMicroelectronics Low power 90nm process) will be then charged into $\overline{Q_m}$ contrarily at the other side, electrons in Q_m will be discharged into Gnd (**Figure 4 (b)**).

Finally, after the charging and discharging process, two transistors MP0 and MN1 are closed, Q_m connects with Gnd via MN0 and $\overline{Q_m}$ connects with

V_{dd_logic}via MP1(**Figure 4 (c)**). Therefore the output of the amplifier then restores a digital level Q_m and $\overline{Q_m}$ whose value depends on the bit stored in the pair of MTJs.

$$I_1 = I_0 + I_2 \quad (1)$$

$$I_4 = I_0 + I_3 \quad (2)$$

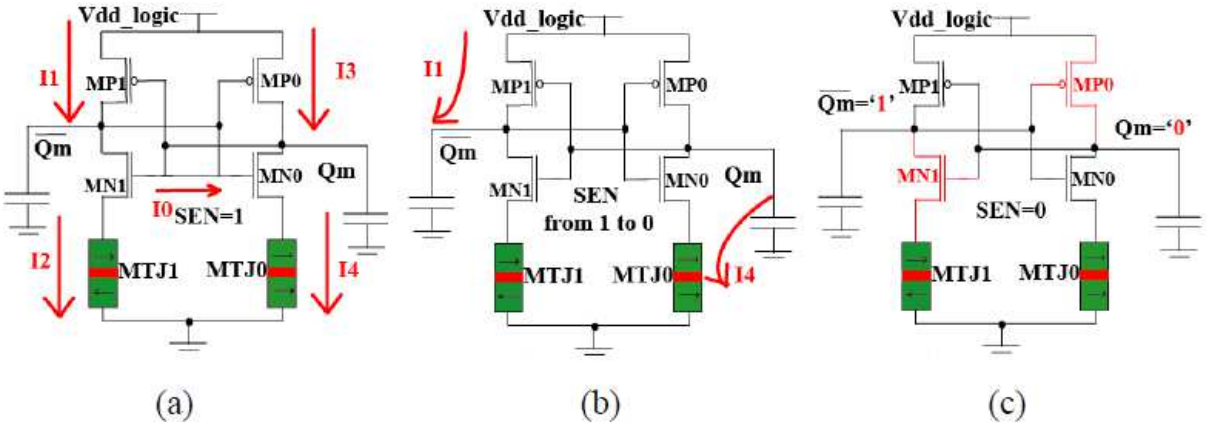

Figure 4: Three states of SRAM based Sense Amplifier (SA). **(a)** Balancing state and $Q_m = V_{dd\_logic}/2$. **(b)** Metastable state is discharging. **(c)** Sensed stable state and shows logic '0' value.

The transient simulation of an STT-TAS MTJ based reading circuit is presented in **Figure 5**. The two MTJs are in two opposite states; one in parallel (red) and the other in the anti-parallel (black) state. When $SEN = 1$, the two outputs Q_m(blue) and $\overline{Q_m}$ (green) are both equal to ~ 370mV; it's the instable state. When $SEN = 0$, the two outputs tend to 0 V and 1 V respectively as expected.

2.2 Switching circuits: Bi-directional current generator

No matter which writing approach, bi-directional current is required in hybrid MTJ/CMOS logic designs to switch the spin direction in the storage layer of MTJ device. SRAM based sense amplifier allows the reading circuit in low power and low area, as a result the MTJ writing circuit occupies the main power and surface of the whole hybrid MTJ/CMOS logic circuit, especially for TAS and FIMS writing approaches which require a switching current more than 1mA.

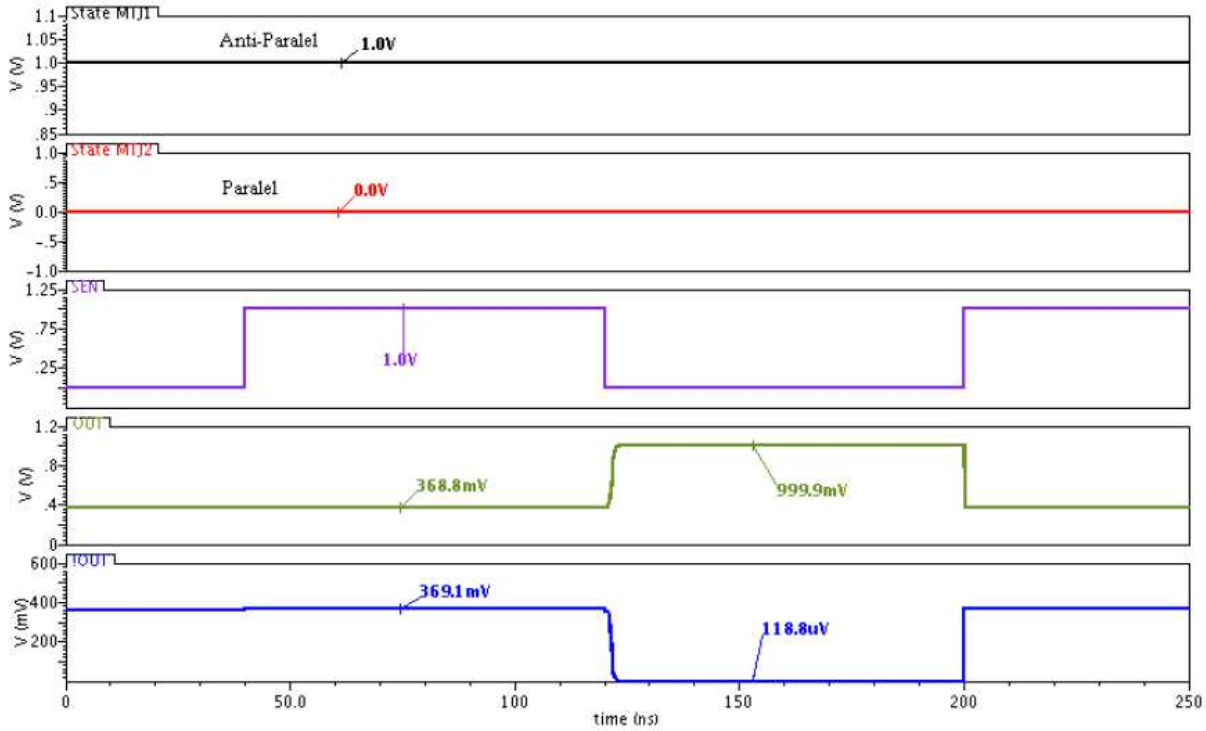

Figure 5: Transient response of an STT-TAS MTJ based reading circuit.

4 NMOS transistor structure has been designed (**Figure 6**) as the main circuit to generate the current in dual direction, where there are always two transistors open and the others closed. In order to generate highest current but consume

lowest area, Only NMOS transistors are used here because PMOS transistors present more and more resistive property than NMOS as the CMOS process technology shrinking; not like V_{dd_logic} used in the sense amplifier, V_{dda} is an analog voltage source, which can be varied and set with a high voltage value (e.g. 5 V). Gnda is also different from Gnd, which needs larger metal surface to pass through higher current.

Another part of the bi-directional current generator is the circuit identifying the current direction in the above structure. Moreover “Enable” signal is absolutely necessary to control the total power, sometimes “Clk” signal is integrated to synchronize the input, “NOR” gates are then applied here to bring these functions with “Input”. **Figure 7** shows a full writing schematic example for

STT writing approach and those for other writing methods or applications are slightly different.

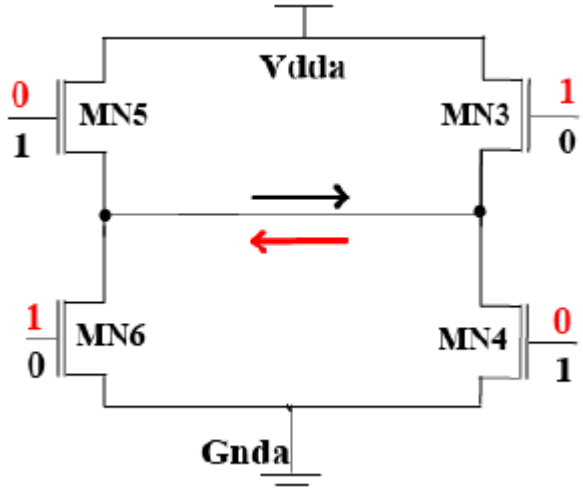

Figure 6: 4T Bi-directional writing structure (MTJ represented by the two opposite arrows).

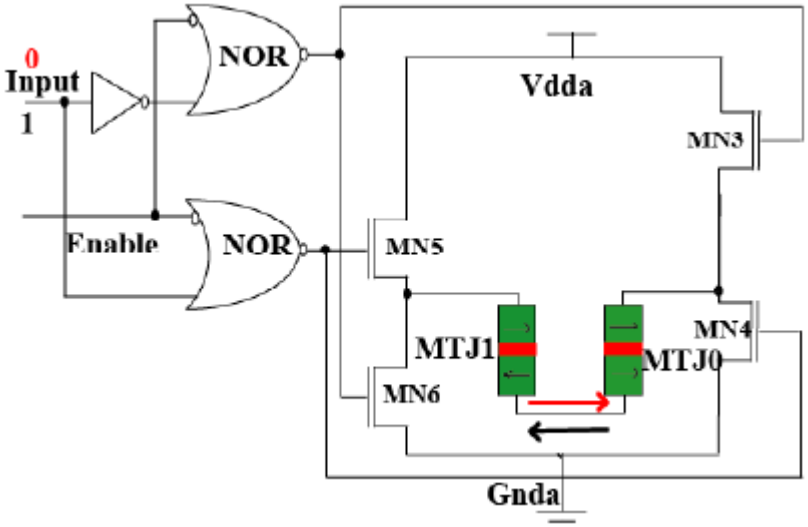

Figure 7: Full writing schematic for STT writing approach.

Two transient simulations where we modified either feeding voltage V_{g1}(applied to MN4 and MN5) and V_{g2}(applied to MN3 and MN6) or transistors dimensions (W: width and L: length) are presented in **Figure 8** and **Figure 9**. The value of the current I_d at the output of each transistor is given by:

$$I_d = \frac{K}{2} * \frac{W}{L} * (V_G - V_T)^2 \qquad with\ K\ and\ V_T\ constants$$

We can notice that we have to make a compromise. Indeed, if we prefer using small transistors (simulation 1), the energy consumption (black and grey) must be higher to reach the coercive (threshold) current (green) and temperature (red), ~ 150 µA and 423 K respectively. Then, the MTJ state switches (blue and purple).

In the other hand, if we prefer using bigger transistors (simulation 2), the energy consumption to reach the critical current and temperature will be lower but the surface will be higher.

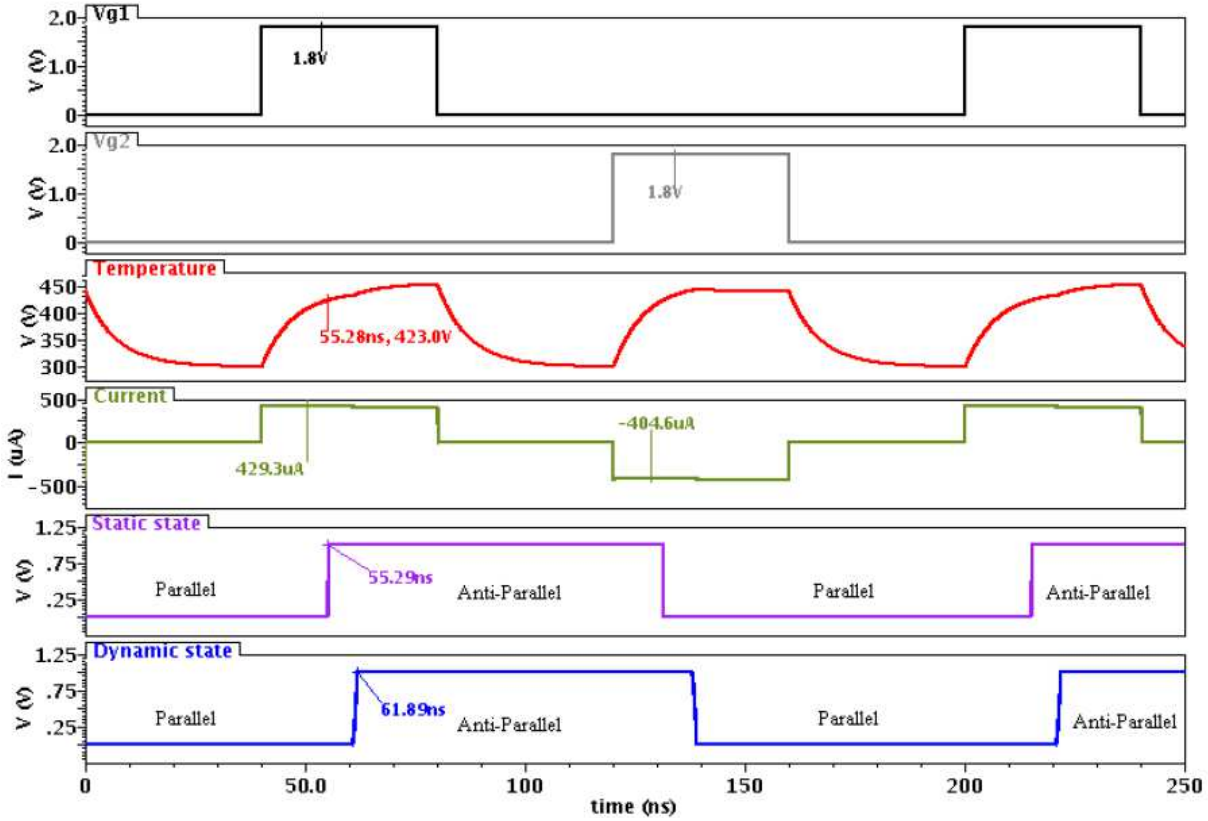

Figure 8: Simulation 1: $V_{g1} = V_{g2} = 1.8\,V$ and $W/L = 650\,nm/65\,nm = 10$.

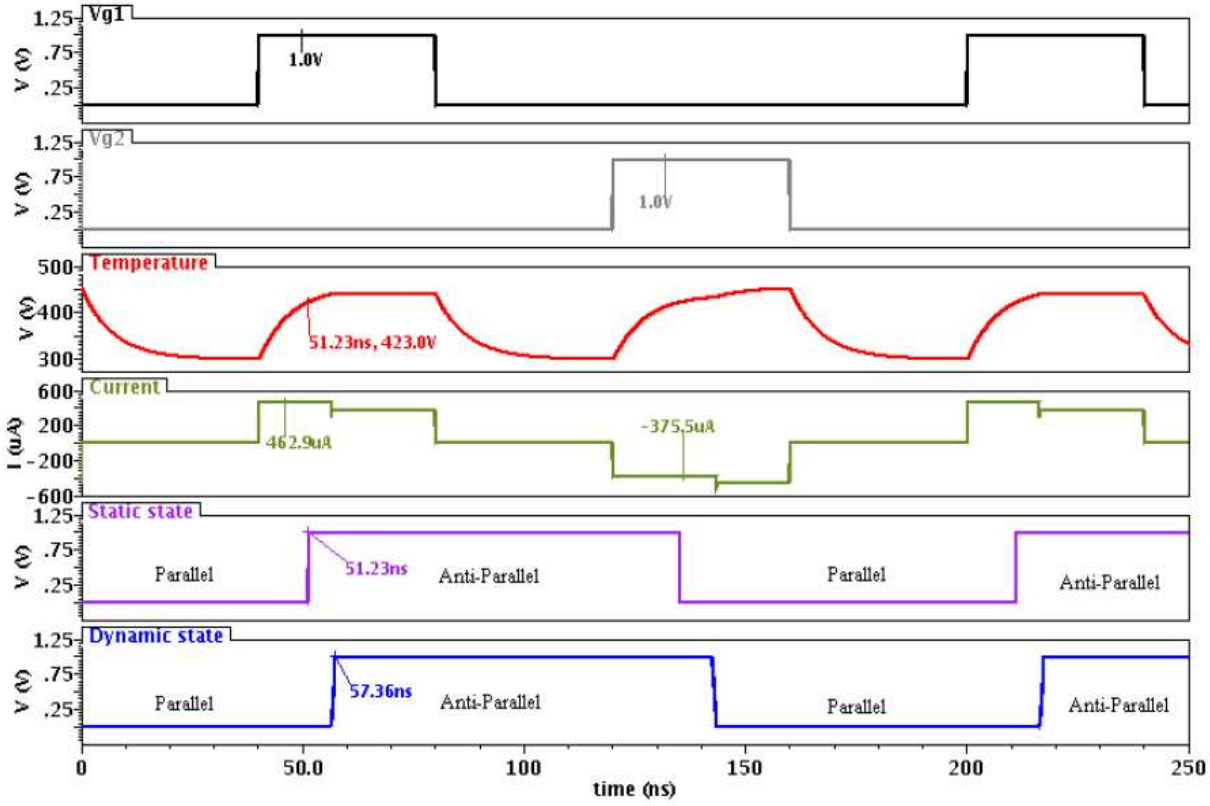

Figure 9: Simulation 2: $V_{g1} = V_{g2} = 1\,V$ and $W/L = 5000\,nm/65\,nm = 77$.

References

[1] C. Chappert, Albert Fert, and F. N. V. Dau, Nat. Mat.6,813 (2007).

[2] S. Sanvito, Nat. Nanotechnol. 2, 204 (2007).

[3] I. Appelbaum, B. Huang, and D. J. Monsma, Nature 447, 295 (2007).

[4] E. Y. Tsymbal, K. D. Belashchenko, J. Velev, S. S. Jaswal, M. V. Schilfgaarde, I. I. Oleynik, and D. A. Stewart, Prog. Mater. Science 52, 401 (2007).

[5] A. N. Chantis, K. D. Belashchenko, D. L. Smith, E. Y. Tsymbal, M. V. Schilfgaarde, and R. C. Albers, Phys. Rev. Lett. 99, 196603 (2007).

[6] International Technology Roadmap for Semiconductors (ITRS), Process Integration, Devices and Structures. (2007)

[7] *InTech Carbon Nanotube Based Thin Films Synthesis and Properties Pdf Free Ebook Download*, n.d. http://ebookbrowse.com/intech-carbon-nanotube-based-thin-films-synthesis-and-properties-pdf-d257366273.

[8] M. Durlam, P. Naji, A. Omair, M. DeHerrera, J. Calder, J. M. Slaughter, B. Engel, N. Rizzo, G.Grynkewich, B. Butcher, C. Tracy, K. Smith, K. Kyler, J. Ren, J. Molla, B. Feil, R. Williams, S. Tehrani "A low power 1Mbit MRAM based on 1T1MTJ bit cell integrated with Copper Interconnects", VLSI Symposium, 2002, USA, pp.158-161.

[9] W. C. Black Jr. and B. Das "Programmable logic using giant-magneto-resistance and spin-dependent tunneling devices" J. Appl. Phys., Vol. 87, No. 9, May, 2000, pp: 6674 -6679

CHAPTER 4: FERROELECTRIC TUNNEL JUNCTIONS

Chapter 4: Ferroelectric Tunnel Junctions

1. Introduction

It has been shown that it is possible to achieve high off/on ratios, and very low write powers using ferroelectric barriers in tunnel junction instead of classical oxide insulators used in precedent magnetic tunnel junctions (MTJs) [1]. Researchers also try to solve a long-standing controversy about the relative importance of electron tunnelling and ionic effects in these devices.

"The operation of the atomic switch relies on the formation of a conductive filament in a metal-oxide insulator sandwiched between two metal electrodes or contacts: this filament forms when a voltage is applied across the electrodes and gives rise to the ON state [2]. The resistive RAM has a similar structure, with oxygen-vacancy-assisted conduction being responsible for the ON state [3, 4]." [13]

The magnetic tunnel junction also has a similar structure, with magnetic electrodes. To switch between states of an MTJ, we apply a magnetic field. At the ON state, the magnetizations of the electrodes are parallel which leads to a high tunnelling current through the device but at the OFF state the magnetizations of the electrodes are anti-parallel which means in this case a low tunnelling current [5, 6].

Using ferroelectric thin films (FTFs) as tunnel barriers, ferroelectric tunnel junctions (FTJs) with polarization switching show important electronic transport properties, such as giant electroresistance [7, 8], giant piezoresistance [9] and non-destructive read out [10]. Many of them present attractive prospects for applications in the functional design of nanotransducers, nonvolatile RAMs, nanodiodes and other nanoferroelectric devices. [11]

2. Ferroelectric tunnel junctions (FTJ)

FTJ seen in **Figure 1** consists of a thin layer (yellow) of ferroelectric material sandwiched between two metal electrodes (blue and green) and the overall potential barrier (solid black line in **Figure 4**) seen by the electrons that tunnel through the ferroelectric layer is the sum of three separate potentials [12, 13]:

- The potential barrier created by the ferroelectric insulator.
- The electronic potential of the two metal electrodes.
- The electrostatic potential introduced by applying an external bias across the device.

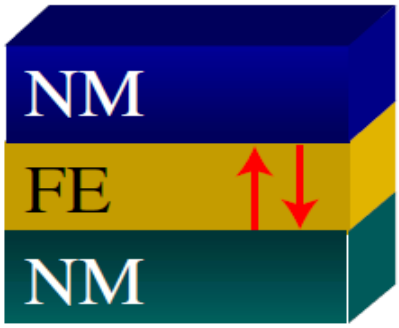

Figure 1: Schematic of a ferroelectric tunnel junction (FTJ). (After ref. [14])

3. The spontaneous polarization and the GER effect in FTJs

Ferroelectrics have a spontaneous polarization P_s, which is nonzero even in the absence of applied electric field (bias voltage). When a ferroelectric and a metal make contact, the spontaneous polarization in the ferroelectric is influenced by the screening effect due to electrons in the metal. Consequently, the basic characteristics of the device will change due to the Thomas–Fermi screening length. Usually for most metals this screening length ranges from 0.01 nm to 0.1 nm [15].

The reversal of the electric polarization in the ferroelectric produces a change in the electrostatic potential profile across the junction. This leads to the resistance change which can reach a few orders of magnitude for metal electrodes with

significantly different screening lengths. This phenomenon is designated as the *giant electroresistance* (GER) effect.

The change of the electrostatic potential profile $\varphi(z)$ induced by the reversal of the electric polarization P in the ferroelectric is the physical mechanism which is responsible for the GER in FTJs. Indeed, if the ferroelectric film is sufficiently thin but still maintains its ferroelectric properties, the surface charges in the ferroelectric are not completely screened by the adjacent metals and therefore the depolarizing electric field in the ferroelectric is not zero [16].

The electrostatic potential associated with this field depends on the direction of the electric polarization. If an FTJ is made of metal electrodes which have different screening lengths, this leads to the asymmetry in the potential profile for the opposite polarization directions. Hence, the potential seen by the transport electrons changes with the polarization reversal [12]. This last one leads to the GER effect: ratio of the two states resistance (or conductance) expressed by the following equation:

$$GER = \frac{R_{off}}{R_{on}} = \frac{G_{on}}{G_{off}}$$

The polarization P creates surface charge densities $\pm \sigma_p = \pm |P|$, on the two surfaces of the ferroelectric film. These polarization charges $\pm \sigma_p$, are screened by the screening charge per unit area $\mp \sigma_s$, which is induced in the two metal electrodes, as is shown schematically in **Figure 2**.[12]

As mentioned before, the different electrodes in an asymmetric FTJ (A-FTJ) break the inversion symmetry of the FTJ. Due to this asymmetric structure, the spontaneous polarization should be expressed as $P_+$and P_- (**Figure 3 (a)** and **(b)**). [11]

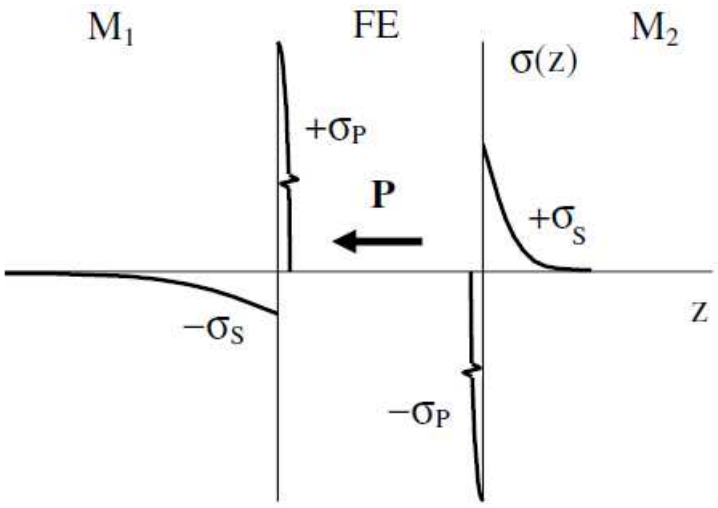

Figure 2: Electrostatics of a M1-FE-M2 junction: charge distribution. (After ref. [12])

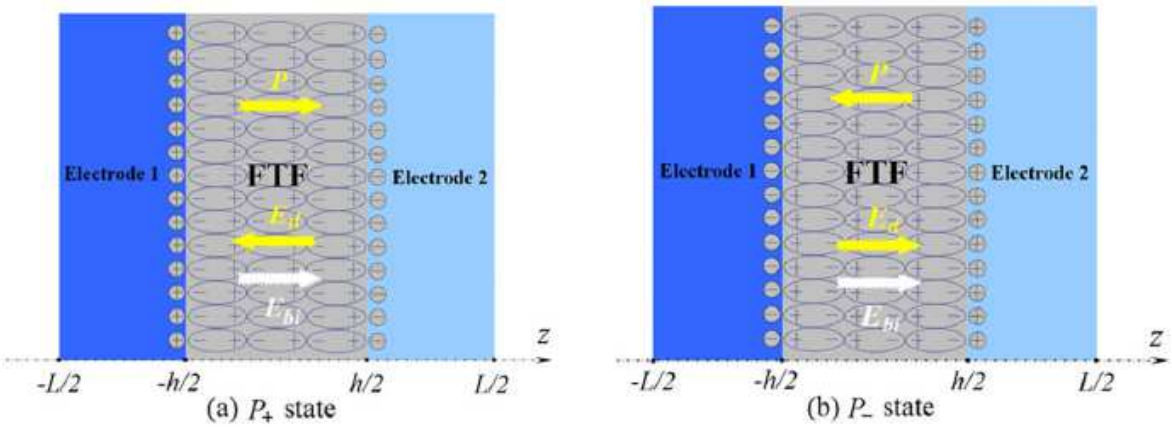

Figure 3: Schematic configuration of an A-FTJ; the arrows denote the directions of the spontaneous polarization P, depolarization field Ed and built-in electric field Ebi. **(a)** P_+ state. **(b)** P_- state. (After ref. [11])

Without an applied electric field, the internal electric field in the FTJ can be derived via Maxwell's equations, and is only related to the depolarization field E_d (equation 1) [11]. The depolarizing electric filed is caused by the polarization charges on the surface of the ferroelectric thin film. The depolarizing field and the spontaneous polarization are oriented in opposite direction as shown in **Figure 3**. [15]

For an A-FTJ, the built-in field E_{bi} (equation 2) due to difference between the work function steps of the two ferroelectric–electrode interfaces has to be considered [17, 18-20]. Then, the total electric field E (equation 3 and 4) in the

ferroelectric thin film (FTF) of the A-FTJ is the sum of the built-in electric field E_{bi} and depolarization field E_d. [11]

$$E_d = -\frac{1}{\varepsilon_b} * \left(1 - \frac{\frac{h}{\varepsilon_b}}{\frac{l_{s1}}{\varepsilon_{e1}} + \frac{l_{s2}}{\varepsilon_{e2}} + \frac{h}{\varepsilon_b}}\right) * P = -\frac{1}{\varepsilon_b} * (1-\theta) * P \quad (1)$$

$$E_{bi} = -\frac{\Delta\varphi_2 - \Delta\varphi_1}{h} = -\frac{\delta\varphi}{h} \quad (2)$$

$$E_+ = E_{bi+} + E_{d+} = -\frac{\delta\varphi}{h} - \frac{1}{\varepsilon_b} * (1-\theta) * P_+ \quad (3)$$

$$E_- = E_{bi-} + E_{d-} = \frac{\delta\varphi}{h} - \frac{1}{\varepsilon_b} * (1-\theta) * P_- \quad (4)$$

Parameter	Description	Default Value
ε_b	The dielectric constant of the background material.	$50*\varepsilon_0$
ε_0	Vacuum permittivity.	$8.85*10^{-12}$F/m
h	The Ferroelectric Thin Film (FTF) thickness.	$2*10^{-9}$ m
ε_{e1}	The dielectric constant of the Electrode 1.	
ε_{e2}	The dielectric constant of the Electrode 2.	
l_{s1}	The screening length in Electrode 1.	
l_{s2}	The screening length in Electrode 2.	
P	The spontaneous polarization.	
$\Delta\varphi_1$	The work function step for ferroelectric-electrode 1 interface.	
$\Delta\varphi_2$	The work function step for ferroelectric-electrode 2 interface.	
$\delta\varphi$	The difference between the work function steps.	
Variable	Description	Default Value
E	The total electric field in the FTF.	
E_d	The Depolarizing field.	
E_{bi}	The Built-in field.	

However and I have to note it, this total field expressed by equations above and given by Zheng,Y and co-workers [11] doesn't fit perfectly with experimental results. I have to remind you too that we are considering ferroelectric thin film barriers of some nanometres thickness (1-5 nm) and in this scale there are other

physical phenomenon not considered yet. Then, we are obliged to wait for new publications about experimental results, expected after July 2012, to have a better comprehension and to be closer to the correct total electric field. This last one will allow us to determine the coercive (threshold) voltage of ferroelectric tunnel junctions and then the switching time (~ 10-20 ns and may be lower, it depends on the applied voltage) which is assumed to depend on the bias and coercive voltage.

The FTJ model I am working on would be completely ready only if we accomplish the static and the dynamic switching models based on finding the conductance equations, the coercive voltage and the switching time, respectively.

4. The ferroelectric thickness limit

"The question of whether or not there is a ferroelectric minimum in lateral dimensions and in thickness is a subject of ongoing discussion for more than 30 years. The pursuit for miniaturization in micro and nanotechnology is a challenge that requires the knowledge and understanding of how reduced dimensions affect the physical properties of a particular material."[21]

"Generally speaking, the most important and useful characteristic of an FTJ is the orders of magnitude change in the tunnelling conductance displayed by it in response to moderate changes in the polarization in the tunnel barrier. Naturally, the stability of ferroelectricity in the FTF is crucial to all these wonderful possibilities. It is well known that ferroelectricity in an FTF can only be retained above the critical thickness h_c [17, 22-24], below which the spontaneous polarization disappears. Obviously, a large critical thickness necessarily puts some rather stringent limitations on the practicality of many novel designs in the nanoregime involving ferroelectric materials.

A good understanding of the factors governing the critical thickness might thus help us to go a long way towards the full utilization of FTJs in nanodevices.

Early studies of the critical properties of FTFs with symmetric electrodes gave the impression that the critical thickness was a few tens of nanometres [24]. More recent experiments and theoretical calculations have found that the critical thickness is much smaller. For example, Tybell *et al* [25] demonstrated the presence of a stable polarization in a 4 nm epitaxial FTF. Tenne *et al* [26] found that the critical thickness of the strained FTF is about 1.6 nm. Fong *et al* [27] observed ferroelectricity of an epitaxial FTF down to 1.2 nm. First principles calculations also predicted that the critical thickness of FTFs could be down to just a few lattice parameters [28-31]. Using the thermodynamic approach, Wang and Woo [32] have derived explicit expressions for the critical thickness of FTFs." [11]

5. The FTJ's state switching

In the absence of an applied electric field, the ferroelectric layer is not polarized and there is a square potential energy barrier of height ϕ_0 (dashed black lines; left panels of **Figure 4**) between the electrons in the two metal layers.

When a negative voltage is applied to the top contact (**Figure 4 (a)**) the ferroelectric layer becomes polarized, with the polarization *P* (green arrow, left panel; dipoles represented by six short arrows, right panel) pointing towards the top electrode and the average height of the potential barrier (solid black line) decreases to ϕ_L (dotted black line), which increases the tunnelling current (red arrow) to give the ON state. When a positive voltage is applied (**Figure 4 (b)**), the polarization of the ferroelectric layer is reversed, the average height of the potential barrier increases to ϕ_H (dotted black line), and the tunnelling current becomes smaller to give the OFF state. E_F is the Fermi level of the top contact.

The ratio R_{off}/R_{on} defines the efficiency of tunnelling electrical resistance (TER) effect. [13]

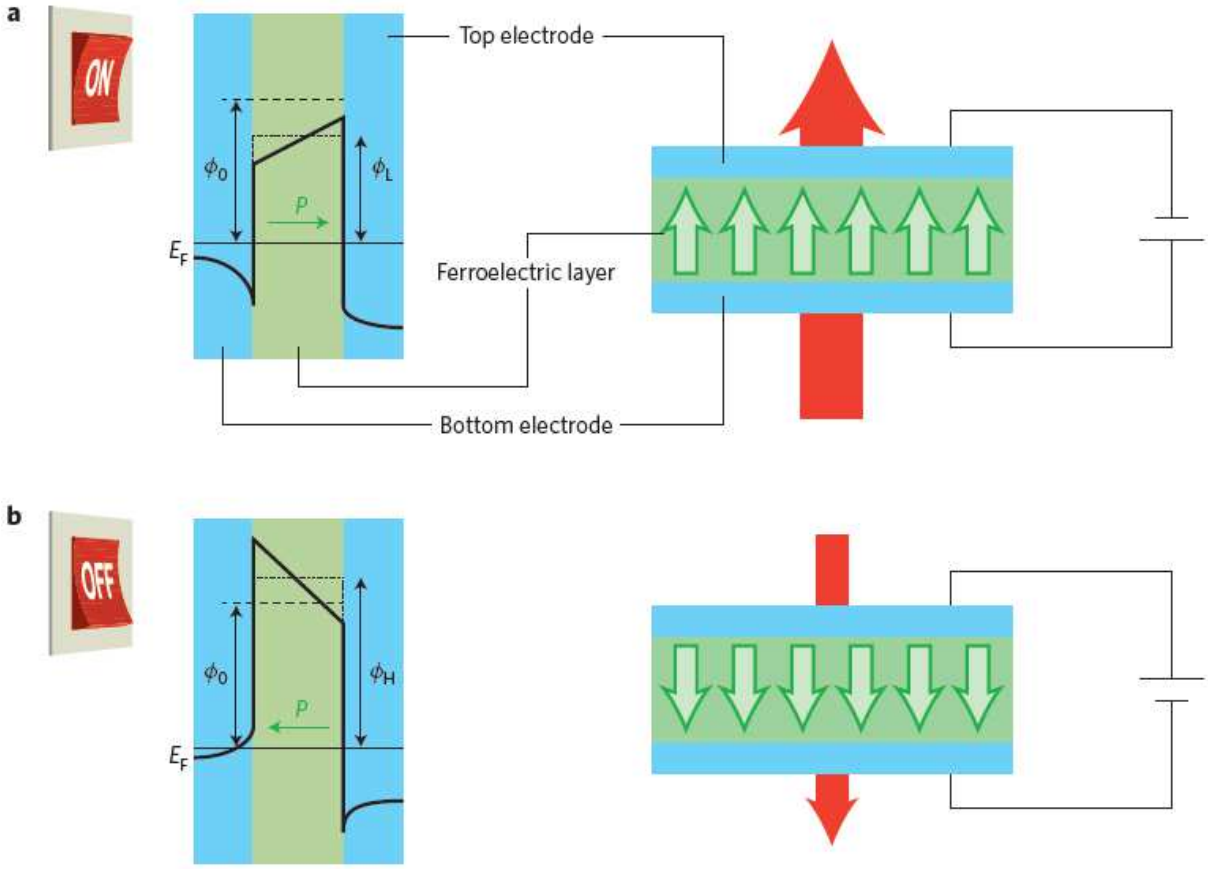

Figure 4: The schematic of a ferroelectric tunnel junction cell when an external voltage is applied to the top contact; (**a**) The ON state. (**b**) The OFF state. (After ref. [13])

Inspired by the polar switch concept that was first proposed by Leo Esaki and co-workers in 1971 [33], interest in ferroelectric tunnel junctions has grown over the past decade. Room-temperature tunnelling electroresistance [34] was first reported in 2003, and this phenomenon has subsequently been explored in more detail using a variety of methods [12, 35-36], including combinations of various scanning force microscopy techniques [37, 38].

The mechanism responsible for resistance switching in ferroelectric tunnel junctions is fundamentally different from that observed in the various magnetic approaches. In particular, it does not require any ionic transport: rather, the electrical resistance of a ferroelectric tunnel junction is determined by the

quantum tunnelling of electrons through the thin ferroelectric layer [13]. This tunnelling rate depends on the height of the potential energy barrier in the device, which can be increased or decreased by the applied electric field (generated by the bias voltage) (**Figure 4**).

The practical challenges associated with this approach are related to scaling (preserving and exploiting ferroelectricity in ultrathin films), controlling the leakage currents, and distinguishing the ferroelectric tunnel electroresistance (tunnelling effects) from changes in the resistance caused by other effects [13].
The France–UK–US collaboration — led by Vincent Garcia of the CNRS, Thales and the Université Paris-Sud — started with a conducting $NdGaO_3$ substrate, and then deposited a 30-nm-thick layer of manganite $La_{0.67}Sr_{0.33}MnO_3$ (LSMO), followed by a 2-nm-thick layer of the ferroelectric material $BaTiO_3$(BTO) and finally, Co/Au contacts (**Figure 5**). LSMO is a half-metallic ferromagnet that is widely used as a ferromagnetic electrode in spintronic devices (because it can achieve almost 100% spin polarization of electrons passing through it), but it is used in this work because the ultrathin BTO layer in the LSMO/BTO sandwich filling is fully strained and has excellent ferroelectric properties.

The electrical characteristics of the resulting memory cell were investigated by grounding the substrate and using the tip of an atomic force microscope to bias the top contact with positive and negative voltages. Positive voltages (~ 3 V) oriented the polarization of the ferroelectric layer downwards (to the LSMO), which placed the device in a high resistive state (OFF) by increasing the height of the tunnelling barrier (**Figure 1 (b)**). Negative voltages oriented the polarization upwards, which lowered the tunnelling barrier (**Figure 1 (a)**) and put the device into a low resistive state (ON). The ratio R_{off}/R_{on} had a value of ~100, which is remarkably high and corresponds to a giant tunnel

electroresistance effect of 10,000% at room temperature (300 K) [1]. The memory can be read with a voltage as low as 100 mV. [13]

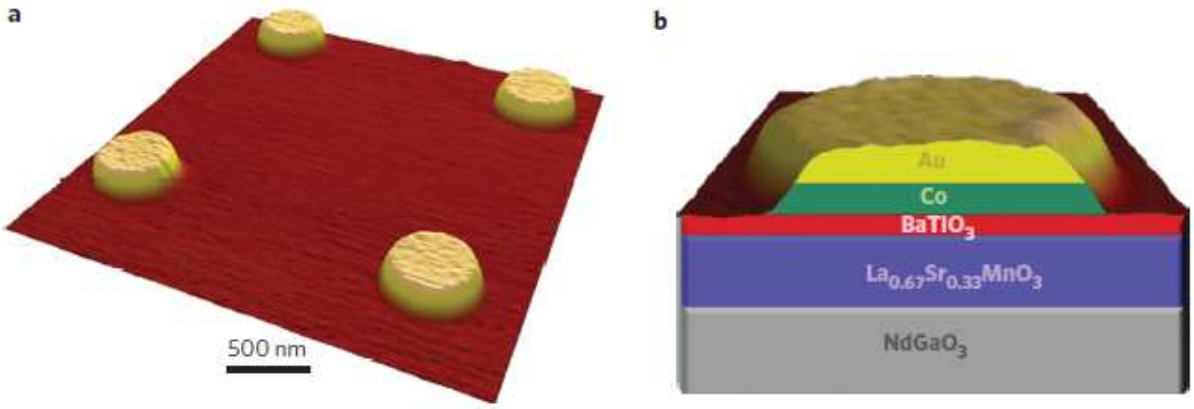

Figure 5: Sketch of the devices. **(a)** Atomic force microscopy (AFM) image of four typical nanodevices defined using electron-beam lithography. **(b)** Schematic of one gold/cobalt/BTO/ LSMO nanodevice on a NGO substrate. (After ref. [1])

Garcia and co-workers argue that the temperature dependence of the measured electroresistance shows that quantum tunnelling is responsible for the current through the BTO layer. However, although they clearly demonstrate the influence of the ferroelectric polarization on the current, they cannot completely exclude the possibility that electrochemical reactions at the interfaces also have a role. Ruling out these other effects will require complementary structural data together with further experiments to investigate what is happening at the interfaces. [13]

One of the major advances reported by Garcia and co-workers is the demonstration of memory programming with short (10 ns) voltage pulses, 3 V in amplitude, and the high reproducibility of the results in a large number of samples. The ferroelectric tunnel junctions show the potential for devices with a low program energy per bit, with experimental values of less than 10 fJ (10 femtojoule) per bit in 50 nm devices: this is less than the typical values for existing flash and phase-change RAM memories (which are in the picojoule to nanojoule range). [1, 13]

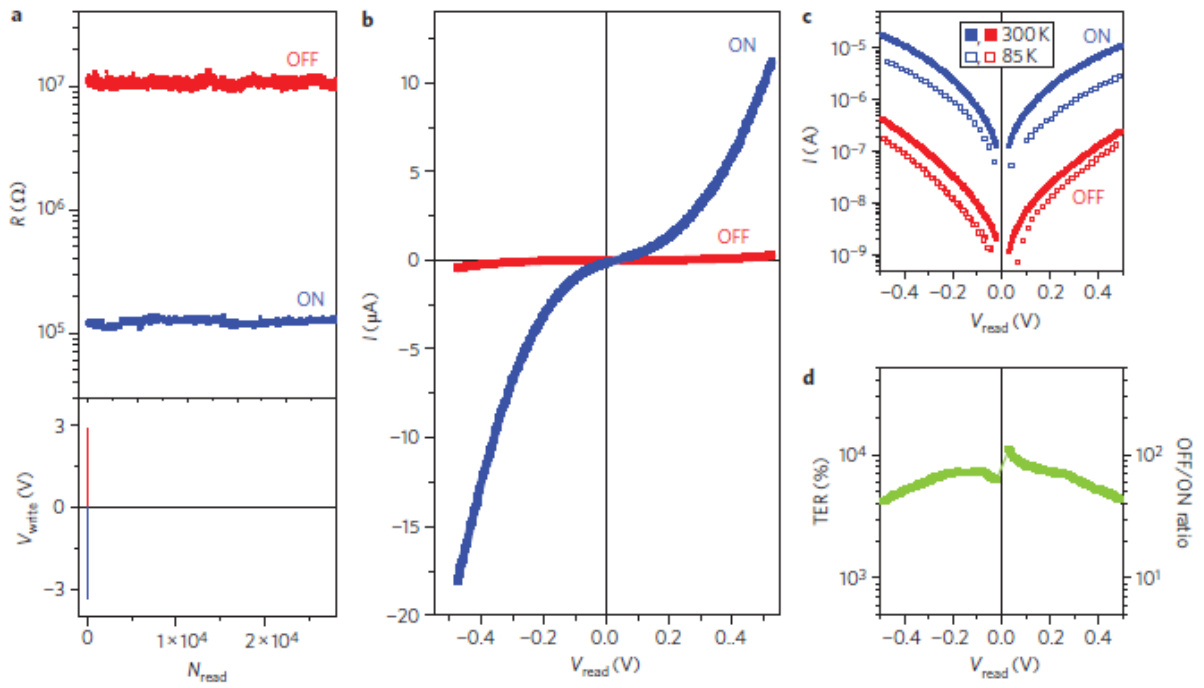

Figure 6: (a) Resistance versus time of a typical device measured at $V_{read} = 100\ mV$ after applying a 100 ms voltage pulse of $+2.9$ V (-3.4 V) to set the OFF (ON) state. **(b)** $I(V_{read})$ for the same device in the ON and OFF states. **(c)** Same $|I(V_{read})|$ in log scale (filled circles) with additional $I(V_{read})$ collected in the ON and OFF states at 85 K (open circles). **(d)** $TER(V_{read})$ calculated from $I(V_{read})$. (After ref. [1])

These latest results represent a basic proof of concept, not a fully optimized memory cell, so a number of challenges remain, such as achieving greater control over the barrier potential and making these devices compatible with siliconsubstrates.

However, it is also clear from this work that quantum tunnelling in ferroelectric materials at the nanoscale offers considerable scope for innovation in nanoelectronic devices.

The purpose of my internship is to find static and dynamic models using equations of the conductance, TER, coercive field and switching time already studied and done. Of course, I always focus and use parameters based on the experimental results reported by Chanthbouala et al ([1]).

References

[1] Chanthbouala, André, Arnaud Crassous, Vincent Garcia, Karim Bouzehouane, Stéphane Fusil, Xavier Moya, Julie Allibe, et al. "Solid-state Memories Based on Ferroelectric Tunnel Junctions." *Nature Nanotechnology* 7, no. 2 (2012): 101–104.

[2] Aono, M. & Hasegawa, T. *Proc. IEEE* **98,** 2228–2236 (2010).

[3] Akinaga, H. & Shima, H. *Proc. IEEE* **98,** 2237–2251 (2010).

[4] Waser, R. & Aono, M. *Nature Mater*. **6,** 833–840 (2007).

[5] Ikeda, S. *IEEE Trans. Electron Devices* **54,** 991–1002 (2007).

[6] Moodera, J. S., Kinder, L. R., Wong, T. M. & Meservey, R. *Phys. Rev. Lett.* **74,** 3273–3276 (1995).

[7] Tsymbal E Y and Kohlstedt H 2006 *Science* **313** 181

[8] Gruverman A *et al* 2009 *Nano Lett.* **9** 3539

[9] Zheng Y and Woo C H 2009 *Nanotechnology* **20** 075401

[10] Garcia V, Fusil S, Bouzehouane K, Vedrenne S E, Mathur N D, Barthelemy A and Bibes M 2009 *Nature* **460** 81

[11] Zheng, Yue, W J Chen, C H Woo, and Biao Wang. "Ferroelectricity in Ultrathin Asymmetric Ferroelectric Tunnel Junctions: Vanishing Critical Thickness." *Journal of Physics D: Applied Physics* 44, no. 9 (March 9, 2011): 095401.

[12] Zhuravlev, M. Ye., R. F. Sabirianov, S. S. Jaswal, and E. Y. Tsymbal. "Giant Electroresistance in Ferroelectric Tunnel Junctions." *Physical Review Letters* 94, no. 24 (June 20, 2005): 246802.

[13] Ionescu, Adrian M. "Nanoelectronics: Ferroelectric Devices Show Potential." *Nature Nanotechnology* 7, no. 2 (2012): 83–85.

[14] Velev, J. P et al. "Multi-Ferroic and Magnetoelectric Materials and Interfaces." *Philosophical Transactions of the Royal Society A: Mathematical, Physical and Engineering Sciences* 369, no. 1948 (August 13, 2011): 3069–3097.

[15] Fasil Kidane. "Multiferroic Tunnel Junctions: Do TER and TMR effects Coexist ?"; Zernike Institute for Advanced Materials, University of Groningen, Nijenborgh 4, 9747 AG Groningen, Then Netherlands (June 2, 2009)

[16] T. M. Shaw, S. Trolier-McKinstry, and P. C. McIntyre, Annu. Rev. Mater. Sci. **30**, 263 (2000).

[17] Zheng Y, Cai M Q and Woo C H 2010 *Acta Mater.* **58** 3050

[18] Pertsev N A and Kohlstedt H 2007 *Phys. Rev. Lett.* **98** 257603

[19] Gerra G, Tagantsev A K and Setter N 2007 *Phys. Rev. Lett.* **98** 207601

[20] Tagantsev A K, Gerra G and Setter N 2008 *Phys. Rev.* B **77** 174111

[21] Contreras, Julio Rodríguez. *Ferroelectric Tunnel Junctions*. Forschungszentrum, Zentralbibliothek, 2004.

[22] Junquera J and Ghosez P 2003 *Nature* **422** 506

[23] Zheng Y, Woo C H and Wang B 2008 *Nano Lett.* **8** 3131

[24] Dawber M, Rabe K M and Scott J F 2005 *Rev. Mod. Phys.* **77** 1083

[25] Tybell T, Ahn C H and Triscone J M 1999 *Appl. Phys. Lett.* **75** 856

[26] Tenne D A *et al* 2009 *Phys. Rev. Lett.* **103** 177601

[27] Fong D D, Stephenson G B, Streiffer S K, Eastman J A, Auciello O, Fuoss P H and Thompson C 2004 *Science* **304** 1650

[28] Stengel M, Vanderbilt D and Spaldin N A 2009 *Nature Mater.* **8** 392

[29] Nunez M and Nardelli M B 2008 *Phys. Rev. Lett.* **101** 107603

[30] Umeno Y, Meyer B, Elsasser C and Gumbsch P 2006 *Phys. Rev.* B **74** 060101

[31] Ponomareva I and Bellaiche L 2008 *Phys. Rev. Lett.* **101** 197602

[32] Wang B and Woo C H 2005 *J. Appl. Phys.* **97** 084109

[33] Esaki, L., Laibowitz, R. B. & Stiles, P. J. *IBM Tech. Discl. Bull.* **13,** 2161 (1971).

[34] Rodriguez-Contreras, J. *et al. Appl. Phys. Lett.* **83,** 4595–4597 (2003).

[35] Tsymbal, E. Y. & Kohlstedt, H. *Science* **313,** 181–183 (2006).

[36] Pantel, D. & Alexe, M. *Phys. Rev. B* **82,** 134105 (2010).

[37] Garcia, V. *et al. Nature* **460,** 81–84 (2009).

[38] Gruverman, A. *et al. Nano Lett.* **9,** 3539–3543 (2009).

CONCLUSION

Tunnel Junctions represent without any doubt the future of memory industry.

Lot of work still remain necessary to develop more these technologies:

- **First,** by understanding better the different reactions and mechanisms in these materials and at the nano-scale.
- **Second**, by finding the best equations which consider most parameters and which are the most coherent with experimental results.
- **Finally**, by designing the best electrical models possible utilizing the best read/write method which deal the best with different compromises and which are of course physically realizable.

APPENDIXES

Appendix A
Introduction to magnetic materials

The origins of magnetism are electron spin and its orbital motion around the atom nucleus.

We consider here the characteristics of magnetic materials when a magnetic field passes through the material. The magnetic moments are arranged in different configurations in different types of materials under an applied field.

The magnetic materials can be classified using some parameters. According to the permeability, magnetic materials can be roughly categorized into three types. If the permeability is slightly less than one (susceptibility slightly less than zero), the material is diamagnetic. If it is slightly greater than one (susceptibility slightly greater than zero), the material is paramagnetic. If it is much more than one (susceptibility much greater than zero), the material is ferromagnetic. However, there also exist some types of magnetic materials that are ferromagnetic or anti-ferromagnetic. **Figure A.1** shows the different kinds of magnetic materials schematically.

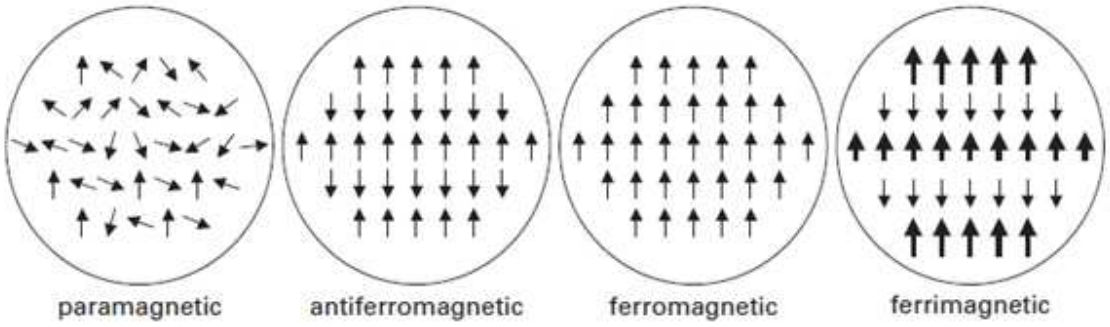

Figure A.1: Ordering of magnetic dipoles in different types of magnetic materials. (After ref. [1])

Reference

[1] DENNY, D. Tang, and Lee Yuan-Jen. *Magnetic Memory: Fundamentals and Technology*. 1st ed. Cambridge University Press, 2010.

Appendix B
Multiferroic and magnetoelectric materials

Glossary of terms
Ferroics: • **Ferroelectric** materials possess a spontaneous polarization that is stable and can be switched hysteretically by an applied electric field; antiferroelectric materials possess ordered dipole moments that cancel each other completely within each crystallographic unit cell. • **Ferromagnetic** materials possess a spontaneous magnetization that is stable and can be switched hysteretically by an applied magnetic field; antiferromagnetic materials possess ordered magnetic moments that cancel each other completely within each magnetic unit cell. • **Ferroelastic** materials display a spontaneous deformation that is stable and can be switched hysteretically by an applied stress. • **Ferrotoroidic** materials possess a stable and spontaneous order parameter that is taken to be the curl of a magnetization or polarization. By analogy with the above examples, it is anticipated that this order parameter may be switchable. Ferrotoroidic materials have evaded unambiguous observation. • **Ferrimagnetic** materials differ from antiferromagnets because the magnetic moment cancellation is incomplete in such a way that there is a net.

A ferroelectric crystal exhibits a stable and switchable electrical polarization that is manifested in the form of cooperative atomic displacements.

A ferromagnetic crystal exhibits a stable and switchable magnetization that arises through the quantum mechanical phenomenon of exchange.

There are very few ‘multiferroic’ materials that exhibit both of these properties, but the ‘magnetoelectric’ coupling of magnetic and electrical properties is a more general and widespread phenomenon [12].

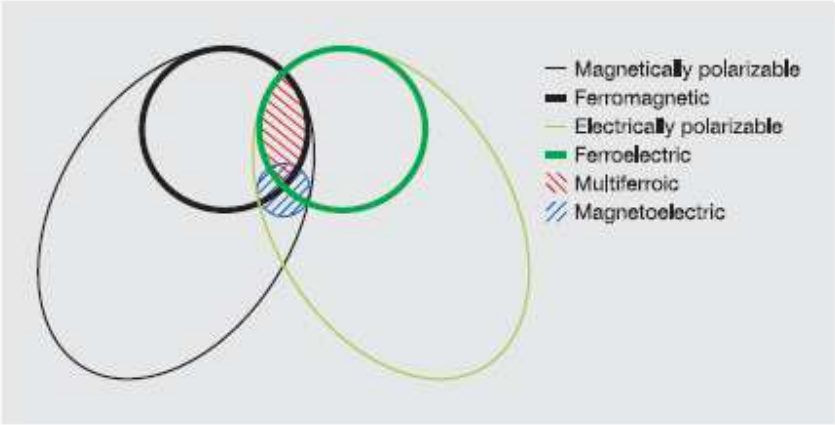

Figure B.1: The relationship between multiferroic and magnetoelectric materials. Ferromagnets (ferroelectrics) form a subset of magnetically (electrically) polarizable materials such as paramagnets and antiferromagnets (paraelectrics and antiferroelectrics). The intersection (red hatching) represents materials that are multiferroic. Magnetoelectric coupling (blue hatching) is an independent phenomenon that can, but need not arise in any of the materials that are both magnetically and electrically polarizable. In practice, it is likely to arise in all such materials, either directly or via strain. (After ref. [12])

Since its discovery less than one century ago, the phenomenon of ferroelectricity [1], like superconductivity, has been considered in relation to the ancient phenomenon of magnetism. Just as recent work has shown that magnetic order can create superconductivity [2], it has also been shown that magnetic order can create (weak) ferroelectricity [3] and vice versa [4,5]. Single-phase materials in which ferromagnetism and ferroelectricity arise independently also exist, but are rare [6]. As this new century unfolds, the study of materials possessing coupled magnetic and electrical order parameters has been revitalized.

It was initially suggested that both magnetization and polarization could independently encode information in a single multiferroic bit. Four-state memory has recently been demonstrated [9], but in practice it is likely that the two order parameters are coupled [10], [11]. Coupling could in principle permit data to be written electrically and read magnetically. This is attractive, given that it would

exploit the best aspects of ferroelectric random access memory (FeRAM) and magnetic data storage, while avoiding the problems associated with reading FeRAM and generating the large local magnetic fields needed to write. Unfortunately, significant materials developments will be required to generate magnetoelectric materials that could make a real contribution to the data storage industry.

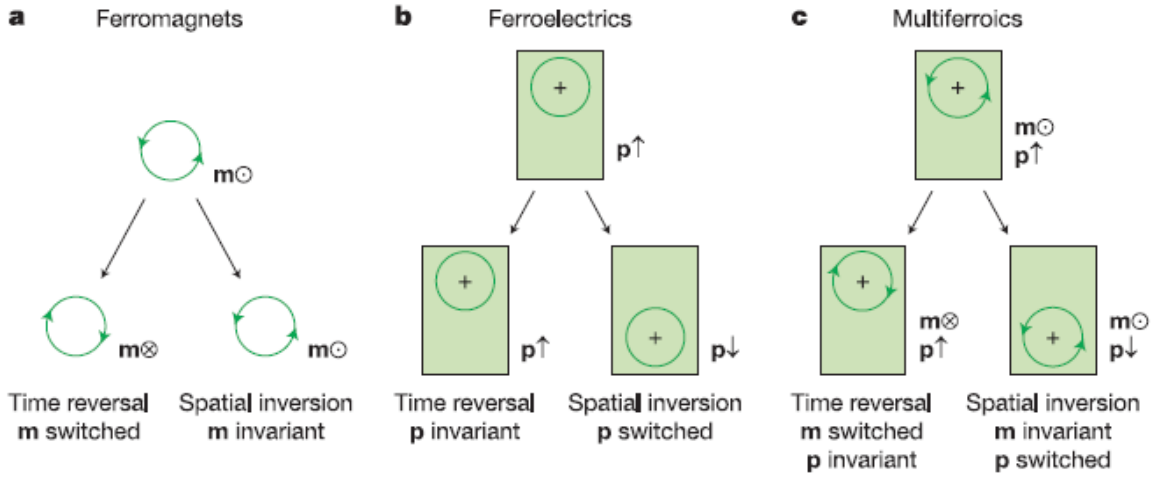

Figure B.2: Time-reversal and spatial-inversion symmetry in ferroics. **(a)** Ferromagnets: The local magnetic moment m may be represented classically by a charge that dynamically traces an orbit, as indicated by the arrowheads. A spatial inversion produces no change, but time reversal switches the orbit and thus m. **(b)** Ferroelectrics: The local dipole moment p may be represented by a positive point charge that lies asymmetrically within a crystallographic unit cell that has no net charge. There is no net time dependence, but spatial inversion reverses p. **(c)** Multiferroics that are both ferromagnetic and ferroelectric possess neither symmetry. (After ref. [12])

"A four-resistance-state device has been obtained, with two states arising from a spin filtering effect due to the ferromagnetic character of the barrier and two resulting from the ferroelectric behavior of the *(*La, Bi*)*MnO3 ultrathin film. These results show that the additional degree of freedom provided by the ferroelectric polarization brings novel functionalities to spintronics, either as an extra order

parameter for multiple-state memory elements, or as a handle for gate-controlled magnetic memories" [13].

With their specificity to exhibit two coupled ferroic orders, multiferroics are a rare class of multifunctional materials. Within the original definition, the class of multiferroic materials only included compounds with two or more ferroic orders but the current trend is to extend it to materials with an antiferroic behavior [12], see **Figure B.3** Ferroelectric materials in which the spontaneous electrical polarization can be switched by the application of an electric field are already largely used in the sensors industry or to design ferroelectric random access memories (FeRAM) in which the information is stored by the remnant polarization [14]. On the other hand, ferromagnetic materials, displaying a spontaneous magnetization that can be reversed by a magnetic field, have been used for a long time for data storage or magnetic field sensors. Furthermore, the research on magnetic multilayers, gave birth twenty years ago to a new electronics called spintronics that takes advantage not only of the charge of the carriers but also of their spins. The incorporation of multiferroic materials in the field of spintronics should allow one to take advantage of both functionalities (for example, ferromagnetism and ferroelectricity) independently but also to add new functionalities due to the coupling between the two orders. This magnetoelectric coupling between magnetism and ferroelectricity opens the way to control of the polarization by a magnetic field or that of the magnetization by an electric field.

This coupling offers interesting perspectives for the design of ferroelectric memories with a non-destructive magnetic reading or magnetic random access memories (MRAM) with an electrical writing procedure (MERAM) [15, 16]. This should open the way to a better integration for these memories thanks to the local

nature of the writing process. Multiferroic materials are scarce and almost all of them are antiferromagnet or weak ferromagnets [17].

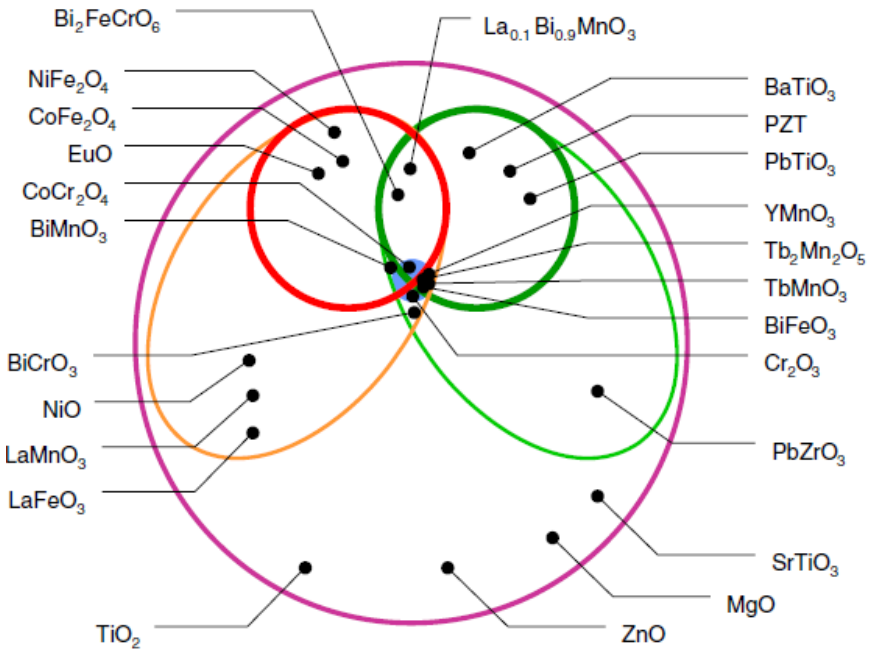

Figure B.3: Classification of insulating oxides. The largest circle represents all insulating oxides among which one finds electrically polarizable materials (green ellipse) and magnetically polarizable materials (orange ellipse). Within each ellipse, the circle represents materials with a finite polarization (ferroelectrics) and/or a finite magnetization (ferro- and ferrimagnets). Depending on the definition, multiferroics correspond to the intersection between the ellipses or the circles. The small circle in the middle denotes systems exhibiting a magnetoelectric coupling. (After ref. [13] and inspired from ref. [12]).

References

[1] Valasek, J. Piezoelectric and allied phenomena in Rochelle salt. Phys. Rev. 15, 537–-538 (1920).

[2] Mathur, N. D. et al. Magnetically mediated superconductivity in heavy fermion compounds. Nature 394, 39–-43 (1998).

[3] Kimura, T. et al. Magnetic control of ferroelectric polarization. Nature 426, 55–-58 (2003).

[4] Scott, J. F. Phase transitions in BaMnF4. Rep. Prog. Phys. 42, 1055–-1084 (1979).

[5] Fox, D. L. & Scott, J. F. Ferroelectrically induced ferromagnetism. J. Phys. C 10, L329–-L331 (1977).

[6] Hill, N. A. Why are there so few magnetic ferroelectrics? J. Phys. Chem. B 104, 6694–-6709 (2000).

[9] Gajek, M. et al. Multiferroic tunnel junctions. Preprint at khttp://arxiv.org/ cond-mat/0606444l (2006).

[10] Schmid, H. On a magnetoelectric classification of materials. Int. J. Magn. 4, 337–-361 (1973).

[11] Ascher, E., Rieder, H., Schmid, H. & Sto¨ssel, H. Some properties of ferromagnetoelectric nickel-iodine boracite, Ni3B7O13I. J. Appl. Phys. 37, 1404–-1405 (1966).

[12] Eerenstein, W., N. D. Mathur, and J. F. Scott. “Multiferroic and Magnetoelectric Materials.” *Nature* 442, no. 7104 (August 17, 2006): 759–765.

[13] Béa, H, M Gajek, M Bibes, and A Barthélémy. “Spintronics with Multiferroics.” *Journal of Physics: Condensed Matter* 20, no. 43 (October 29, 2008): 434221.

[14] Dawber M, Rabe K M and Scott J F 2005 *Rev. Mod. Phys.* **77** 1083.

[15] Bibes M and Barth´el´emy B 2008 *Nat. Mater.* **7** 425.

[16] Chen X, Hochstrat A, Borisov P and Kleeman W 2006 *Appl. Phys. Lett.* **89** 202508.

[17] Hill N A 2000 *J. Phys. Chem.* B **104** 6694.

Appendix C

Time-dependent dielectric breakdown (TDDB) of magnetic tunnel junction devices

The dielectric breakdown characteristics of magnetic tunnel junctions are the primary reliability concern. It has been found that the distribution of time dependent dielectric breakdown (TDDB), t_{BD}, as a function of stress voltage across an MTJ, VMTJ, closely follows the Weibull distribution [1]:

$$F(x) = 1 - \exp\left(-(x/\alpha)^{\beta}\right)$$

In this case, x is the time-to-breakdown, t_{BD} at a given stress voltage; α is the scaling factor between t_{BD} and the stress voltage, V_{MTJ} and β is the activation energy – both are extracted from the Weibull plot. The operating life of a MTJ at a given V_{MTJ} can therefore be projected by constructing a series of Weibull plots of the TDDB of different V_{MTJ} stress voltages, usually greater than the operating voltage. Thus, the tunnel barrier of the MTJ breaks down in a short time.

By measuring the t_{BD} of a large number of MTJs at a stress voltage V_{MTJ}, one obtains the cumulative distribution of $F(t_{BD})$. From $F(t_{BD})$, one may construct one line on the Weibull plot $g(t_{BD}) = \ln\left(-\ln\left(1 - F(t_{BD})\right)\right)$. Repeating the same measurement at a different stress voltage, one can construct another line. **Figure C.1 (a)** shows the Weibull plots of $g(t_{BD})$ of four stress voltages. The slope of the $g(t_{BD})$ data line of each stress voltage is roughly the same. For each stress voltage V_{MTJ}, 63% of the devices break down at a time that each curve intersects at $g(t_{BD}) = 0$. Knowing β, one can project the operating voltage of the MTJ at a breakdown probability of 10^{-12}.

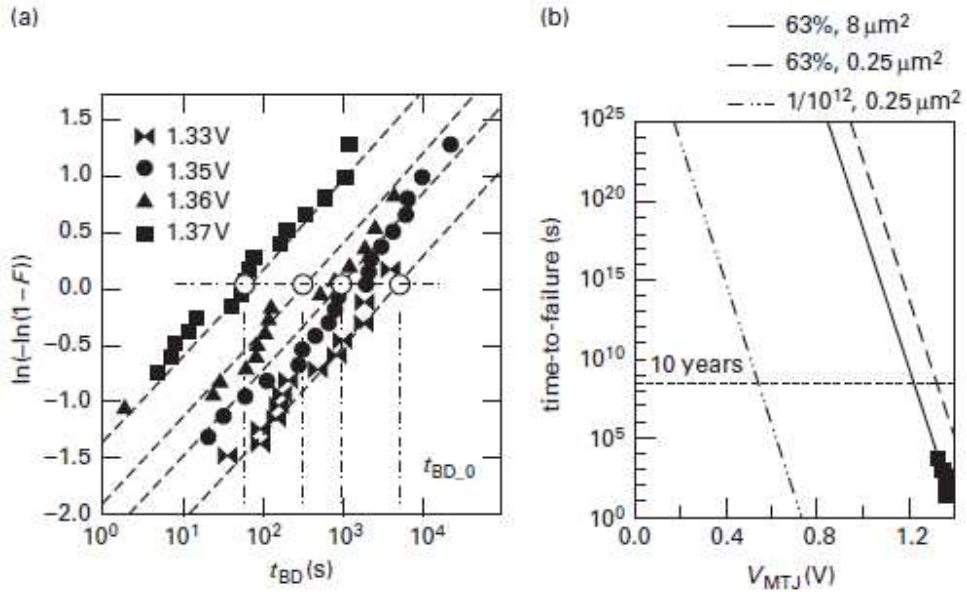

Figure C.1: (a) Weibull plot of time-dependant dielectric breakdown (TDDB) of four different stress voltages; t_{BD_0} is the time at which 63% of the MTJs break down. **(b)** Time-to-failure vs. V_{MTJ}. (After ref. [1])

Reference

[1] J. Das, R. Degraeve, P. Roussel, G. Groeseneken, G. Borghs and J. De Boeck, J. Appl. Phys. 91(10), 7712 (2002).

Appendix D

Unit conversion table for cgs and SI units

Force, F	1 dyne (dyn)	10^{-5} newton (N)
Magnetic field strength, H	1 oersted (oe)	79.58 ampere/meter (A/m)
Magnetic induction, B	1 gauss (G)	10^{-4} tesla (T)
Electric field strength, E	1 erg	10^{-7} joule (J)
Magnetic flux density, Φ	1 maxwell	10^{-8} weber (Wb)
Magnetization, M	1 emu/cm³	$12.57*10^{-4}$ Wb/m² (or A/m)

Appendix E

Dimensions of units of magnetism

SI magnetic units are easily related to the current, voltage and energy in MKS units, since the SI system was originally developed under the assumption that magnetism is originated from electric current. The dimensions of magnetic units are shown below; A = amperes, s = seconds, kg = kilograms and m = meters.

(1) Newton (N) = kg.m/s²;
(2) Joule (J) = kg.m²/s²;
(3) Magnetic field (H) = A/m;
(4) Henry (h) = kg.m²/s².A²;
(5) Tesla (T) = kg/s².A;
(6) Weber (Wb) = kg.m²/s².A.

Magnetism in cgs (centimeter, gram, second) units is less transparent. The unit of magnetic moment m is the emu. The density of the magnetic moment MS is emu/cm3. The magnetic induction is given by $B = H + 4\pi M_s$where the magnetic field H is given in units of oersted (Oe) and B is given in gauss (G).

Appendix F

Physical constants

Symbol	Value (unit)
μ_B (Bohr magneton)	$9.27*10^{-21}$ erg/Oe, $9.27*10^{-24}$ J/T
q (elementary charge)	$1.602*10^{-19}$ C
k_B (Boltzman constant)	$1.38*10^{-34}$ J/K
k_BT/q (Thermal voltage at 300 K)	0.0259 V
h ($Planck\ constatnt$)	$6.626*10^{-24}$ J.s
$\hbar$ (=h/2π, reduced Planck constant)	$1.054*10^{-24}$ J.s
ε_0 (permittivity in a vacuum)	$8.86*10^{-14}$ F/m
μ_0 (permeability in a vacuum)	$1.257*10^{-6}$ H/m

BIBLIOGRAPHY

Bibliography

[1] DENNY, D. Tang, and Lee Yuan-Jen. *Magnetic Memory: Fundamentals and Technology*. 1st ed. Cambridge University Press, 2010.

[2] Contreras, Julio Rodríguez. *Ferroelectric Tunnel Junctions*. Forschungszentrum, Zentralbibliothek, 2004.

[3] BHUSHAN, B. *Springer handbook of nanotechnology*. 3rd ed. Springer, 2010.

[4] *InTech Carbon Nanotube Based Thin Films Synthesis and Properties Pdf Free Ebook Download*, n.d. http://ebookbrowse.com/intech-carbon-nanotube-based-thin-films-synthesis-and-properties-pdf-d257366273.

[5] Floyd, T.L. *Digital fundamentals*. 9th ed. Pearson Perentice Hall, 2006.

[6] MALVINO, A.P. and D.J BATES. *Electronic principles*. 7th ed. The Mc Graw Hill campanies, 2007.